NEOPLASIA
www.neoplasia.com

Volume 13 Number 11 November 2011 pp. 1005–1018 1005

Conditional Expression of Oncogenic C-RAF in Mouse Pulmonary Epithelial Cells Reveals Differential Tumorigenesis and Induction of Autophagy Leading to Tumor Regression[1,2]

Fatih Ceteci*, Jiajia Xu†, Semra Ceteci*, Emanuele Zanucco*, Chitra Thakur* and Ulf R. Rapp*

*Department of Molecular Biology, Max Planck Institute of Biochemistry, Martinsried, Germany; †Department of Physiological Chemistry, Theodor-Boveri-Institute, Biocenter, Würzburg, Germany

Abstract

Here we describe a novel conditional mouse lung tumor model for investigation of the pathogenesis of human lung cancer. On the basis of the frequent involvement of the Ras-RAF-MEK-ERK signaling pathway in human non–small cell lung carcinoma (NSCLC), we have explored the target cell availability, reversibility, and cell type specificity of transformation by oncogenic C-RAF. Targeting expression to alveolar type II cells or to Clara cells, the two likely precursors of human NSCLC, revealed differential tumorigenicity between these cells. Whereas expression of oncogenic C-RAF in alveolar type II cells readily induced multifocal macroscopic lung tumors independent of the developmental state, few tumors with type II pneumocytes features and incomplete penetrance were found when targeted to Clara cells. Induced tumors did not progress and were strictly dependent on the initiating oncogene. Deinduction of mice resulted in tumor regression due to autophagy rather than apoptosis. Induction of autophagic cell death in regressing lung tumors suggests the use of autophagy enhancers as a treatment choice for patients with NSCLC.

Neoplasia (2011) 13, 1005–1018

Introduction

Non–small cell lung carcinoma (NSCLC) is the most prevalent type of lung cancer and is responsible for most cancer-related deaths worldwide [1]. Genetic analysis of human NSCLC has highlighted the mitogenic cascade Ras-RAF-MEK-ERK as a frequent target of mutagenesis [1,2]. In contrast to *K-RAS* mutations that are detected frequently in human lung adenocarcinomas [3], activating mutations in *RAF* genes are not common and are only observed in the *B-RAF* gene at low frequency [4,5]. Despite lack of activating mutations, overexpression of C-RAF was found in most human pulmonary adenocarcinomas [6]. Moreover, C-RAF but not B-RAF has recently been shown to be the RAF family member of serine/threonine protein kinase that is essential for K-*ras* oncogene-driven NSCLC [7]. By now, many of the mitogen-activated protein kinase (MAPK) pathway oncogenes have been examined in mouse models for human NSCLC, which include spontaneous and conditional expression strategies demonstrating a close genetic and histopathogenic relationship [8]. With respect to the cell of origin of NSCLC, a considerable body of data indicated that oncogenic K-Ras generated invariably tumors of type II cell lineage irrespective of whether the expression was targeted to Clara and/or to alveolar type II cells [8]. Whether the tumor-initiating cells also include bronchiolar Clara cells that transdifferentiate to alveolar type II cells or include progenitors of these cells has yet to be elucidated [8].

Address all correspondence to: Fatih Ceteci, PhD, Department of Molecular Biology, Max Planck Institute of Biochemistry, Am Klopferspitz 18, 85152 Martinsried, Germany. E-mail: fceteci@biochem.mpg.de

[1]This study was supported by Deutsche Krebshilfe-Mildred Scheel Foundation (grant 106253) and by the DFG (grants TR17).

[2]This article refers to supplementary materials, which are designated by Figures W1 to W20 and are available online at www.neoplasia.com.

Received 9 May 2011; Revised 7 September 2011; Accepted 8 September 2011

DOI 10.1593/neo.11652

C-RAF fusion transcripts that lost the RAS-binding domain were found in human prostate, melanoma, and liver cancer, suggesting genomic rearrangement rather than mutation as a mechanism of C-RAF gene activation in a subset of solid tumors [9]. Previously, we have shown that constitutive expression of C-RAF BxB, an N-terminal deleted form of C-RAF that lacks RAS-binding domain, or wild-type C-RAF under the control of *SP-C* promoter yields thousands of adenomas that were well differentiated, poorly vascularized, and did not progress to metastasis [10,11]. However, there were several questions that could not be answered with these constitutive models. For example, what is the target cell availability in adult *versus* embryonic lung? Is tumor induction reversible, and if so, by what mechanisms do the tumors regress? How does the range of transformation sensitive target cells compare between the oncogenic C-RAF and K-*ras*? To address these critical questions, we have engineered a novel conditional transgenic mouse line for further investigating the pathogenesis of human NSCLC. Our findings demonstrate that the targeted expression of transgenic C-RAF to alveolar type II cells using *SP-C rtTA* mice led to the development of a limited number of macroscopic lung tumors that did not progress to invasive and metastatic malignancy. Moreover, embryonic or adult expression of oncogenic C-RAF did not alter the number and the quality of the lung tumors indicating the presence of transformation sensitive type II cells in the postnatal lung. Curiously, the expression of oncogenic C-RAF in Clara cells using *CCSP rtTA* mice failed to induce lung neoplasias in most mice, indicating differences in the susceptibility of lung epithelial cells to oncogenic insults. Importantly, tumor maintenance was strictly dependent on the continuous expression of the initiating oncogene as discontinuing transgene expression by withdrawal of doxycycline (DOX) resulted in the regression of adenomas. In contrast to reversible *K-ras*^{G12D} or *B-RAF*^{V600E} lung tumor models [12,13], the mechanism of regression was not associated with apoptosis but involved autophagy. To our knowledge, this is the first *in vivo* evidence to support autophagy as an important cell death pathway in a malignant tissue. These findings are relevant for clinical studies that are aiming to use autophagy enhancers or C-RAF inhibitors as anticancer agents in NSCLC patients.

Materials and Methods

Generation of Transgenic Mice

All animal studies were approved by the Bavarian State authorities for animal experimentation. Mice were housed under barrier conditions in air-filtered, temperature-controlled units with a 12-hour light-dark cycle with free access to food and water. To generate mice conditionally expressing C-RAF BxB [10], pcDNA3 plasmid harboring ha-tagged oncogenic C-RAF, hereafter C-RAF ha-BxB, was digested with *Hin*dIII and *Xba*I and cloned into pTS4 vector. The resulting pTS4-C-RAF ha-BxB plasmid was subsequently cut with *Sma*I and *Xba*I to clone a 1.3-kb C-RAF ha-BxB fragment into pBI5 vector (containing a tet operator) using *Pvu*II (compatible with *Sma*I site) and *Xba*I sites. The final PBI5 C-RAF ha-BxB plasmid was cut with *Ase*I to remove the vector backbone, and the Tet-O C-RAF ha-BxB fragment (6.0 kb) was isolated by gel electrophoresis and injected into the pronucleus of fertilized mouse eggs. We generated eight potential founders, and five of them showed germ line transmission after polymerase chain reaction (PCR) genotyping. All positive founders were mated with either *SP-C rtTA* or *CCSP rtTA* [14] transgenic activator lines to obtain double transgenic progeny. These compound mice were induced with DOX (Sigma, Munich, Germany) containing food (500 mg/kg body weight; Ssniff, Soest, Germany) for different periods and analyzed for the phenotypic occurrence of lung pathologic abnormality. For embryonic induction, DOX was administered to dams from E0.5 onward. All mice were kept on FVB/n background. K-*ras*^{LA2} mice were obtained from the Jackson Laboratory (Bar Harbor, ME) [37].

Genotyping

DNA was extracted from mouse tails and genotyping was performed by PCR. To identify Tet-O C-RAF ha-BxB mice, TETO (5′-GCA GAG CTC GTT TAG TGA ACC) and BxB (5′-ACA TCT CCG TGC CAT TTA CCC) primers were used. Amplification of the PCR product for Tet-O C-RAF ha-BxB was performed as follows: denaturation at 94°C for 2 minutes followed by 37 cycles at 94°C for 15 seconds, annealing at 66°C for 30 seconds and 72°C for 1 minute, followed by a 5-minute extension at 72°C. Genotyping of *SP-C rtTA* and *CCSP rtTA* transgenic mice was previously described [14].

RNA Isolation and Reverse Transcription–PCR Analysis

Total RNA was isolated from whole lungs of mice using TRIzol (Invitrogen, Darmstadt, Germany) reagent. Samples were treated with RNase-free DNAse I before the preparation of complementary DNA (cDNA) using random hexamer primers provided by the First-Strand cDNA Synthesis Kit (Fermentas, Sankt Leon-Rot, Germany). Control reactions were run using Taq polymerase without reverse transcription (RT) enzyme. PCR conditions for amplification of C-RAF BxB were as follows: denaturation at 94°C for 3 minutes followed by 28 cycles at 94°C for 15 seconds, annealing at 56°C for 30 seconds and 72°C for 30 seconds, followed by a 10-minute extension at 72°C. To identify C-RAF BxB, 5′-TGG GCC GAG GAT ATG CCT CCC and 5′-CAA GGA TGG CTC GGA AGC GC primers were used. β-Actin was used to check the quality of the RNA extraction and RT-PCR. The primers and condition for β-actin have been previously described [11]. PCR products were resolved on a 1.5% agarose gel. Real-time RT-PCR was performed using the DyNAmo HS SYBR Green qPCR Kit (Finnzymes, Schwerte, Germany) in a Roto-Gene 2000 detection system (Corbett Research, Hilden, Germany). RNA of hypoxanthine phosphoribosyltransferase 1 (HPRT) was used as a standard control. Antisense primers for transgenic (h) C-RAF, endogenous (m) C-RAF, and their common sense oligo (hm) were as follows: h, 5′-ACATGTGT-TCTGCCTCTGGA-3′; m, 5′-ATGCATTCTGCCCCCAAGGA; hm, 5′-TTTCCCCAGATCCTGTCTTCCAT-3′.

Immunoblot Analysis

For protein analysis of lung samples, mice were killed and their macroscopic lung tumors were collected in tubes containing ice-cold RIPA buffer with protease inhibitor cocktail. Lungs were homogenized for 30 seconds using an ultraturax homogenizer in a cold environment. The homogenates were centrifuged at 11,000 rpm for 10 minutes. After centrifugation, supernatants from samples were analyzed for protein concentration by NanoDrop ND-1000 (Thermo Fisher Scientific, Erlangen, Germany). The remaining extracts were mixed with 4× Laemmli loading buffer heated to 95°C for 5 minutes and either stored at −20°C or resolved by SDS-PAGE and transferred to nitrocellulose membranes. After blocking for an hour in PBS (0.05% Tween, 5% powdered skimmed milk) blots were incubated overnight

with the following primary antibodies: anti-ha antibody (1:500, clone 3F10; Roche, Mannheim, Germany), LC3 (1:250, clone RB7481; Abgent, Surrey, United Kingdom), mammalian kinase target of rapamycin (mTOR, 1:1000, L27D4; Cell Signaling, Frankfurt, Germany), phospho-mTOR (1:1000, Ser2481; Cell Signaling), Raptor (1:1000, 24C12; Cell Signaling), Rictor (1:1000; Cell Signaling), AMPKα (1:1000, F6; Cell Signaling), phospho-AMPKα (Thr172) (1:1000, 40H9; Cell Signaling), $p70^{S6K}$ (1:1000, 49D7; Cell Signaling), phospho-p70S6K (Thr389) (1:1000, 1A5; Cell Signaling), Akt (1:1000, 9272; Cell Signaling), phospho-Akt (Ser473) (1:1000, 193H12; Cell Signaling), Bcl-2 (1:1000, 2876; Cell Signaling), Beclin 1 (1:2500, NB500-249; Novus Biological, Cambridge, United Kingdom), p16 (1:500, sc-1661; Santa Cruz, Offenbach, Germany), p21 (1:500, sc-6246; Santa Cruz), p53 (1:500, sc-126; Santa Cruz), HP-1γ (1:500, clone 42s2; Millipore, Schwalbach, Germany), cyclin D2 (1:500, sc-181; Santa Cruz), cleaved caspase 3 (1:1000, D175; Cell Signaling), PARP (1:1000, 46D11; Cell Signaling), and β-actin (1:5000, I-19; Santa Cruz). After three washes with 1× Tris-buffered saline with 1% Tween 20 buffer, the membranes were incubated with corresponding anti-IgG peroxidase–coupled secondary antibodies (GE Healthcare, Freiburg, Germany) for 60 minutes and visualized with an ECL detection kit.

Histopathology and Immunostaining

Tissues were fixed in 4% buffered formalin for 24 hours and then transferred to 70% ethanol before embedding in paraffin. Six-micrometer-thick mouse tissue sections were cut from paraffin-embedded blocks, placed on glass slides. The cut slides were deparaffinized, rehydrated in a graded series of alcohol, and haematoxylin-eosin (H&E) stained using standard procedures. For immunohistochemistry, sections were deparaffinized and rehydrated. For antigen retrieval, sections were incubated in 10 mM citrate buffer for 10 to 20 minutes using microwave irradiation. Endogenous peroxidase activity was quenched with methanol or PBS containing 1% to 3% H_2O_2. Nonspecific binding was blocked with 5% of serum with 0.2% Triton X-100 for 1 hour. After blocking, sections were incubated with primary antibodies overnight at 4°C. Primary antibodies against the following proteins were used: aquaporin 5 (AQP-005; Alomone Labs, Jerusalem, Israel) at 1:1000, CCSP (sc-9772; Santa Cruz) at 1:2500, pan-Cytokeratin (Z0622; Dako, Hamburg, Germany) at 1:500, Ki67 (MM1; Vector Laboratories, Lörrach, Germany) at 1:50, pro–SP-C (gift from Jeffrey A. Whitsett), TTF-1 (M3575; Dako) at 1:100, vimentin (C-20; Santa Cruz) at 1:200, E-cadherin (clone ECCD2; Zymed Laboratories, Darmstadt, Germany) at 1:250, Pecam-1 (clone MEC 13.3; BD Pharmingen, Heidelberg, Germany) at 1:100, F4/80 (ab6640; Abcam, Cambridge, United Kingdom) at 1:100, phospho-p44/p42 MAPK Thr202/Tyr204 (20G11; Cell Signaling) at 1:1000, Raf-1 (E-10; Santa Cruz) at 1:400, ha-tag (3F10; Roche) at 1:200, active caspase-3 (5A1E; Cell Signaling) at 1:200, LC3 (clone RB7481; Abgent) at 1:100, phospho-mTOR (2448, 49F9; Cell Signaling) at 1:200, p53 (CM5; Vector Laboratories) at 1:200, CD3 (ab5690; Abcam) at 1:250, p16 (sc-1661; Santa Cruz) at 1:50, p21 (sc-6246; Santa Cruz) at 1:200, and HP-1γ (clone 42s2; Millipore) at 1:200. After primary antibody incubation, sections were incubated with corresponding biotinylated secondary antibodies (Dako Cytomation, Hamburg, Germany) at a 1:200 dilution for 60 minutes at room temperature. ABC reagent was applied (Vectastain Elite ABX Kit; Vector Laboratories) and developed in diaminobenzidine (DAB). Sections were then counterstained with hematoxylin and mounted after dehydration. Phospho–p44/p42 MAPK staining was essentially carried out as the others except that Tris-buffered saline with 1% Tween 20 was used instead of PBS. For immunofluorescence staining, the following secondary antibodies (all obtained from Jackson ImmunoResearch Laboratories, at 1:200 dilutions) were used: donkey anti-mouse Cy3, donkey anti-mouse Cy5, donkey anti-goat Cy5, donkey anti-goat Cy3, donkey anti-rabbit Cy3, donkey anti-rabbit Cy5, donkey anti-rabbit Alexa 488, donkey anti-rat Cy3, and donkey anti-rat Cy5. Masson trichrome staining was carried out according to Sigma-Aldrich's instruction for trichrome stain (Masson) kit (Sigma; cat. no. HT15), which stains nuclei in black; cytoplasm, muscle, and erythrocytes in red, and bone/collagen in blue. To quantify the multiplicity of LC3+ foci/tumors, we counted the number of LC3-positive cells per five randomly selected tumor areas for each tumor. At least five tumors were counted for each lung tumor section. We used three mice for each time point. Apoptotic cells were identified using the Dead End Fluorometric TUNEL-Kit (Promega, Mannheim, Germany) according to the manufacturer's instructions. Scoring for Ki67- or TUNEL-positive cells was carried out by counting the number of positive nuclei per field in 10 randomly chosen tumor regions at 40× magnification. Approximately 500 to 1500 nuclei were screened per each field. For each condition, all data from three to four separate mice were pooled to obtain final cell numbers. Further evaluation of apoptosis was carried out by analyzing internucleosomal cleavage of DNA. For genomic DNA isolation, lung tumors were digested using Gentra Puregene Tissue Kit (158622; Qiagen, Hilden, Germany) according to the manufacturer's instructions. Genomic DNA isolated from mouse MLE-15 NSCLC cells (using Gentra Puregene Cell Kit (158388; Qiagen) that were treated either with cycloheximide (5 μg/ml, C4859; Sigma) or with doxorubicin hydrochloride (2 μg/ml; Fisher Bioreagents, Schwerte, Germany) for 24 hours were used as positive controls. For the analysis of H&E staining and immunohistochemistry, we used Zeiss Axio Scope. A1 or Zeiss Discovery V8 Streo microscopes (Carl Zeiss MicroImaging GmbH, Göttingen, Germany) integrated with AxioCam ICc3 camera (Spectra Service, Ontario, NY). Images were acquired using AxioVision Rel. 4.7 software provided by Zeiss. Negative controls included the omission of the primary antibody. Macroscopic lung lesions were counted before fixation.

Statistical Analyses

Differences among the groups were compared with Student's *t* test using GraphPad Prism 5 software (GraphPad Software, Inc, San Diego, CA). Results are presented as means ± SEM. All *P* values were 2-tailed. Survival and tumor incidence were analyzed by the log-rank test. $P < .05$ was considered statistically significant.

Results

Generation of Mice with a Conditional C-RAF Oncogene

To generate mice in which we could regulate the expression of oncogenic C-RAF (C-RAF BxB) in respiratory epithelial cells, the tet-regulated construct (Tet-O C-RAF ha-BxB) was prepared as described in the Materials and Methods section. After screening of genomic DNA from pups, we have obtained six transgenic mouse founders that showed positive germ line transmission for the insert. To facilitate detection of transgene expression, an ha-tag was added to the N-terminal part of the oncogenic C-RAF (Figure 1*A*). Each founder was crossed with a *SP-C rtTA* activator mouse line that directs rtTA expression into alveolar type II cells [14] to obtain double-transgenic (DTR) mice. The resulting DTR mice (hereafter referred

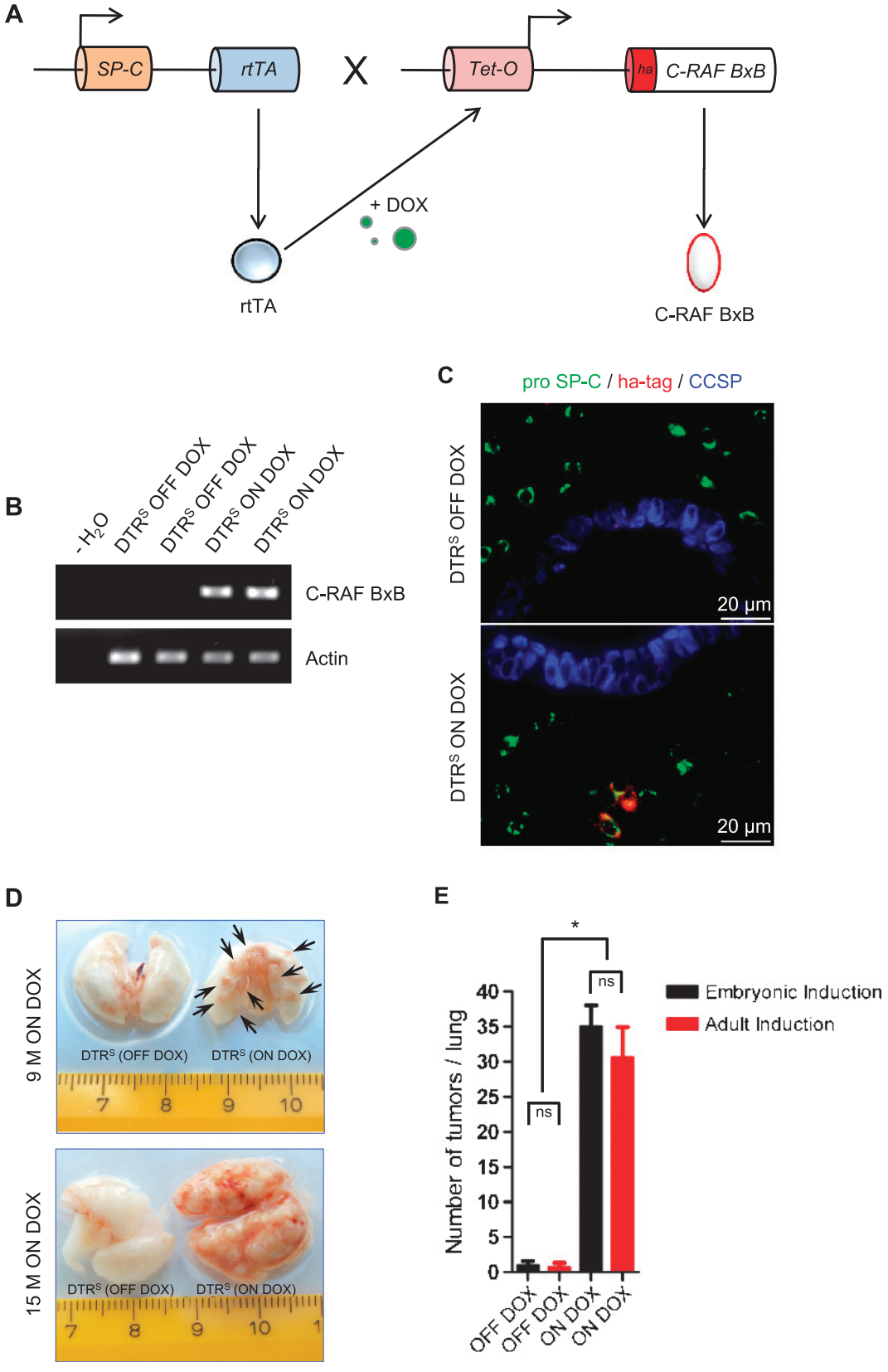

Figure 1. Inducible expression of oncogenic C-RAF in alveolar type II cells leads to macroscopic lung tumor development. (A) Schematic representation of the constructs for conditional expression of oncogenic C-RAF in type II pneumocytes. (B) RT-PCR analysis of total lung samples prepared from DTR^S mice demonstrates oncogenic C-RAF transcript only in induced mice. (C) Triple immunofluorescence staining of lung sections from DTR^S mice for the indicated antibodies showing oncogenic C-RAF expression (arrows) in a fraction of alveolar type II cells after DOX treatment. (D) Photographs of representative lungs with multiple macroscopic pulmonary nodules (arrows). (E) Quantitation of lung tumors in embryonic and adult induced DTR^S mice. Error bars are SEM from eight different mice for each category. NS indicates not significant. *Statistically significant ($P < .05$).

to as DTR^S where "S" stands for *SP-C rtTA*) were then placed on a continuous DOX diet at 5 weeks of age for a period of 4 to 6 months and killed for pathologic examination. Histologic examination of lung sections from induced DTR^S mice showed lung tumors in two (founder numbers; 3579 and 2393) of the six founders (Figure W1). On the basis of larger tumor size and longer latency (2 *vs* 4-5 months), a feature of human NSCLC, we first selected founder number 2393 for the subsequent experiments (Figure W1). To determine the transgene expression, 5-week-old DTR^S mice were DOX treated for 1 week and analyzed by semiquantitative RT-PCR and by immunofluorescence staining. RT-PCR analysis of total lungs from induced and control DTR^S mice showed oncogenic C-RAF expression only in induced mice demonstrating tight regulation of transgene expression (Figure 1*B*). Consistent with the site of expression of the human *SP-C* promoter [15], oncogenic C-RAF expression judged by ha-tag staining was found in a fraction of alveolar type II cells but not in bronchiolar Clara cells of the induced DTR^S mice (Figure 1*C*).

Expression of Oncogenic C-RAF in Alveolar Type II Cells Elicits Multiple Macroscopic Lung Tumors

In contrast to our previous constitutive RAF transgenic mouse model (SP-C C-RAF BxB), in which thousands of microscopic adenomas were formed [10], adult induction of oncogenic C-RAF in type II pneumocytes generated visible macroscopic lung tumors albeit at low number and longer latency (Figure 1*D*). To test whether the discrepancy in the observed tumor incidence between the two strains was associated with the time course of induction, we next prolonged DOX treatment of adult DTR^S mice to 9 and 15 months, respectively. Interestingly, incidence and size of the tumors increased with continued exposure to DOX (Figure 1*D*). Despite higher tumor burden in long-term-induced adult DTR^S mice, the number of pulmonary tumors was still low in comparison with the constitutive model. We therefore had to consider that the number of transformation-sensitive cells targeted by the oncogenic C-RAF differs during and after lung development. To test this hypothesis, DTR^S mice were either prenatally or postnatally exposed to sustained DOX induction during a 9-month period. To our surprise, quality and multiplicity of macroscopic lung tumors did not differ between embryonic and adult induction (Figure 1*E*). Taken together, these data show that oncogenic C-RAF is a potent initiator of lung tumors originating in alveolar type II cells and the number of target cells available for transformation is independent of developmental age.

Lack of Tumor Progression in Macroscopic Lung Tumors

With respect to histopathology, induced pulmonary tumors were alveolocentric and composed of a monomorphous population of cells arranged in a ribbon pattern with no nuclear pleomorphism (Figure 2*A*). Tumors contain minimal stroma consisting of collagen fibers (Figure W2) and displayed lepidic growth along alveolar septa without tissue destruction (Figure 2*A*). Similar to the constitutive C-RAF transgenic mouse model, we did not detect focal hyperplasia at all ages analyzed. Consistent with oncogenic C-RAF expression judged by ha-tag staining, tumor cells showed strong C-RAF and nuclear phospho-ERK1/2 expression (Figure 2*B*). Similar to $B\text{-}RAF^{V600E}$– or K-ras^{V12}–driven murine lung tumors where tumor cells progressively showed diminished proliferation and gained the features of senescence [16–18], tumor cells fueled by oncogenic C-RAF showed reduced nuclear staining of Ki67 and heterogeneous expression of HP-1γ, $p21^{WAF1}$, and $p16^{INK4a}$ (Figure W3, *A* and *B*). Notably, we often found increased active macrophage accumulations around the tumors but not intratumorally (Figure W4*A*). In contrast to macrophages, T cells were frequently detected in the tumors (Figure W4*B*).

To ascertain the cell type and differentiation status of the tumors, immunohistochemistry was performed using antibodies against Clara cell antigen (CCSP) and the surfactant protein C (SP-C), commonly used markers that distinguish between Clara cells and alveolar type II cells, respectively. All of the lung tumors were found to be positive for pro–SP-C and negative for CCSP, implicating alveolar type II cells as the origin of these lesions (Figure W5). We detected homogenous nuclear TTF-1 expression as well as heterogeneous expression of aquaporin 5 in tumors (Figure W5). Consistent with the lack of invasive edges, tumor cells did not show evidence for epithelial-mesenchymal transition as judged from the sustained expression of epithelial markers such as Pan-cytokeratin, E-cadherin (Figure W6*A*), and negative expression of the mesenchymal marker Vimentin (Figure W6*B*). In agreement with our previous results [11], pulmonary tumors initiated by adult expression of oncogenic C-RAF were generally poorly vascularized and showed low density of blood vessels only at the tumor periphery (Figure W7*A*). Lack of angiogenic induction was also maintained in tumor nodules larger than 1.5 mm diameter (Figure W7*B*). Despite their benign characteristics, we went on to examine whether tumors with this striking macroscopic appearance gave rise to metastasis. Intensive histopathologic inspection of large cohorts of mice did not reveal any micrometastases or macrometastases in the regional lymph nodes or in distant organs (Figure W8). On the basis of all these histologic criteria, we concluded that induced tumors driven by oncogenic C-RAF are well differentiated and do not progress to malignancy, thus classifying them as adenomas. These data also clearly implicate that tumor size is not necessarily a criterion for malignancy.

Clara Cell–Targeted Expression of Oncogenic C-RAF Results in Rare Lung Tumor Formation

We next wanted to evaluate oncogenic C-RAF for its ability to transform Clara cells. To meet this goal, Tet-O C-RAF ha-BxB single-transgenic mice were bred with the *CCSP rtTA* inducer line to obtain DTR mice (hereafter referred to as DTR^C where "C" stands for *CCSP rtTA*) (Figure W9*A*). Similar to DTR^S mice, we readily detected transgene messenger RNA (mRNA) expression in induced mice (Figure W9*B*). Consistent with the sites of expression of the rat *CCSP* promoter [19–21], expression of ha-tag was detected both in Clara cells and in the alveoli (Figure W9*C*). To determine tumorigenic effects of oncogenic C-RAF in Clara cells, adult DTR^C mice were kept under continuous DOX for different time points. In contrast to DTR^S mice, pathologic inspection of large cohorts of DTR^C mice during long-term DOX stimulation did not reveal visible lung lesions in most mice even when we prolonged the induction for 18 months (Figure 3, *A* and *B*). Lack of pulmonary nodules in DTR^C mice was not a function of the maturity of Clara cells as embryonic induction also gave rise to similar results (Figure 3*B*). Moreover, tumor-bearing DTR^S mice died at the expected rate [22], whereas DTR^C mice survived for the entire induction period (Figure 3*A*). Histologic examination of lung sections from induced DTR^C mice showed the absence not only of pulmonary tumors but also of Clara cell hyperplasia (Figure 3*C*). Only in a minority (3/32) of the induced DTR^C mice between the ages of 12 and 18 months, we found a low number of macroscopic lung tumors

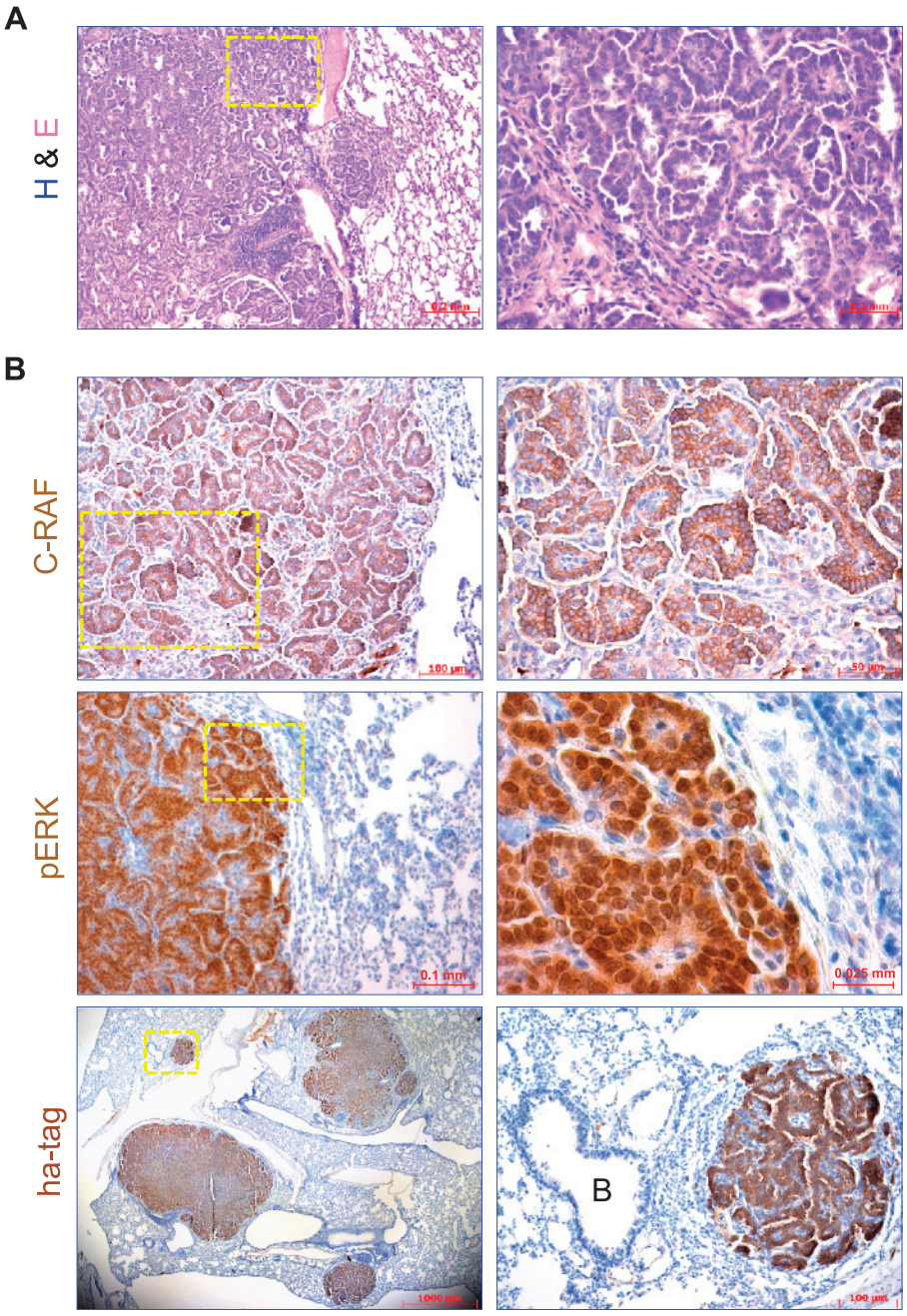

Figure 2. Histopathologic analysis of lung tumors induced by oncogenic C-RAF. (A and B) Lung sections from 15-month-induced DTR^S mice were stained with the indicated markers. Pictures in the right-hand panel are the higher-magnification views of the boxed areas (yellow) shown in left panels. Hematoxylin (blue) was used as a counterstain.

(Figure 3*D*). These tumors were indistinguishable from those found in DTR^S mice in their macroscopic appearance and histology (Figure 3*D*). As in the case of DTR^S mice, lung tumors were not bronchiolocentric and found to be positive for pro–SP-C and negative for CCSP, suggesting that these lesions arose from alveolar type II cells or their precursors (Figure 3*D*).

To address whether differential tumorigenicity between the DTR^S and DTR^C mice related to the level of transgene expression, we compared mRNA levels by real-time RT-PCR. We found similar levels of oncogenic C-RAF expression between the mice groups (Figure W9*D*). As such, comparison of transgene mRNA levels to endogenous expression of C-RAF gave rise to identical results between DTR^S and DTR^C mice (Figure W9*E*). Failure to induce lung neoplasia in most of the induced DTR^C mice might be related to the choice of the founder line (founder 2393) because there are examples of idiosyncratic properties of single founder strain lines. We therefore established similar mating using another mouse founder line (founder 3579) that responds to oncogenic C-RAF expression with lung tumor formation with relative early latency (Figure W1). Toward this aim, DTR mice both from *SP-C rtTA* (referred as DTR^{S2} where "2" indicates the second founder) and *CCSP rtTA* (referred as DTR^{C2}) crosses were induced with DOX for 3.5 months

of period. As expected, examination of the lung slides from DTR^{S2} mice showed multiple pulmonary adenomas (Figure W10, *A* and *B*). Consistent with their transgene origin, all the lung tumors expressed ha-tag and stained positive for pro–SP-C but not for Clara cell marker CCSP, attesting to alveolar type II cell origin (Figure W10*C*). Similar to DTR^{C} mice, DTR^{C2} mice also failed to develop lung tumors and showed generally normal bronchiolar structures (Figure W10, *B* and *D*). Distinct from DTR^{C} mice, we found bronchiolar hyperplasias in a minor fraction (1%-2%) of the induced DTR^{C2} mice (Figure W11*A*). Such hyperplastic lesions were never found in control

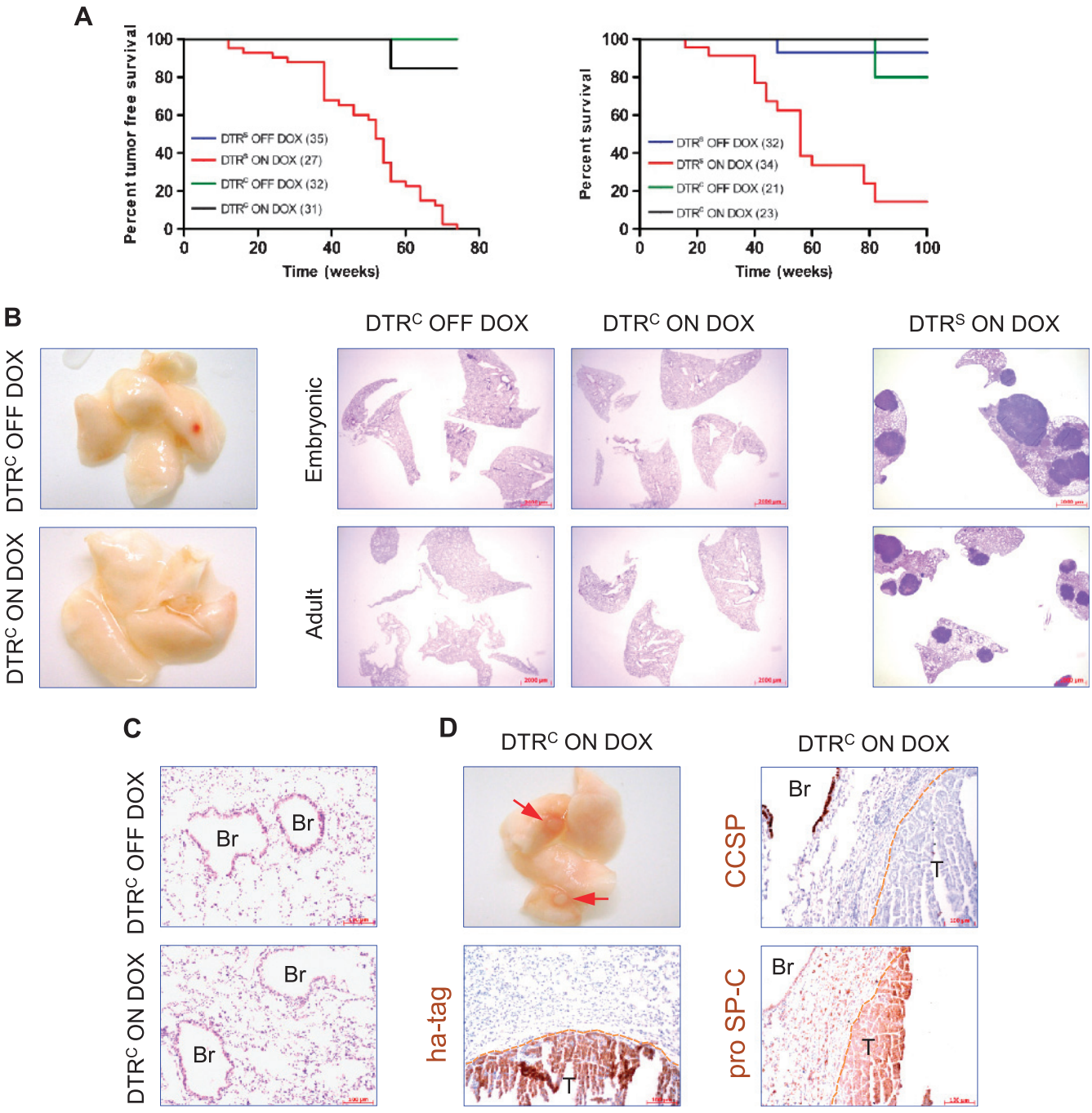

Figure 3. Differential tumorigenicity between type II pneumocytes and Clara cells targeted by active C-RAF. (A) Kaplan-Meier curves for lung tumor incidence and survival with the indicated genotypes. Animal numbers are as indicated. DOX-treated DTR^{S} mice display statistically significant (log-rank analysis) tumor penetrance associated with reduced life span compared with their counterparts. (B) Photographs of lungs and their representative pictures of H&E-stained sections from DTR^{C} mice showing lack of lung tumors after long-term (13 months) DOX induction compared with age-matched DTR^{S} mice. (C) Representative H&E-stained lung sections from control and induced (13 months) DTR^{C} mice showing normal bronchiolar morphology. (D) Photograph of lung isolated from a 13-month-induced DTR^{C} mouse showing pulmonary tumors (red arrow) and their immunohistochemical characterization with the indicated markers. Br indicates bronchiole; T, tumor.

DTR^{C2} mice. The rare bronchiolar hyperplasias arising within the terminal bronchioles displayed papillary excrescences (Figure W11*B*). Unexpectedly, this hyperplastic epithelium stained negative for CCSP but positive for pro–SP-C, suggesting a transdifferentiation event toward alveolar lineage (Figure W11*B*). Lack of lung tumors derived from bronchiolar Clara cells was not due to the induction of premature senescence because we did not observe $p19^{ARF}$ or $p16^{INK4a}$ expression in ha-tag–expressing Clara cells of the DTR^{C} mice (data not shown). Taken together, these results indicate that lung epithelial cells targeted by the rat *CCSP* promoter are strongly refractory to oncogenic C-RAF–driven neoplastic transformation.

Oncogenic C-RAF Is Essential for Tumor Maintenance

To assess the dependence of lung tumors on oncogenic C-RAF for survival and continued growth, tumor-bearing DTR^{S} mice (induced for 8 months) were taken off the DOX diet for 1 month. Macroscopic inspection of whole lungs from deinduced mice showed strong reduction in tumor burden with few persistent lesions remaining after DOX withdrawal (Figure 4*A*). To assess the early effects of DOX withdrawal on tumor phenotype, DOX was removed from mice carrying established tumors at different time points. After 3 days of DOX withdrawal, we did not observe any histologic alterations in the tumor cell morphology in comparison with the control cells (Figure 4*B*). However, after 1 week, we detected a significant reduction in staining intensity (H&E) in central tumor sections, which was even more pronounced after 2 weeks of DOX removal while maintaining tumor structure (Figure 4*B*). The pale tumor cells disappeared gradually and were replaced by normal-looking pulmonary tissue (Figure 4*B*). Staining of lung sections with an ha-tag antibody paralleled the histologic observations and showed diminished transgene expression gradually after DOX withdrawal (Figure 4*C*). Notably, both collagen fibers and T cells that are present in the stroma of control (ON DOX) tumors (Figures W2*A* and W4*B*) completely disappeared after discontinuing transgene expression (Figures W12 and W13). Interestingly, we detected a dramatic loss of pro–SP-C expression in the regressing lung tumors indicating a dedifferentiation process (Figure W14, *A* and *B*). These data indicate that maintenance of lung tumors and their stromal components requires continuous expression of oncogenic C-RAF.

To address the mechanism of tumor regression, we first focused on the involvement of cell cycle arrest in lung tumors removed from the DOX. We found that the shutdown of oncogenic C-RAF expression from the induced lung tumors caused reduced cell proliferation as evident by a substantial decrease of Ki67-positive cells (Figure W15, *A* and *B*). Reduction of cyclin D2 levels in regressing lung tumor lysates supported this finding (Figure W15*C*). Another cell autonomous mechanism that restricts tumor growth is oncogene-induced senescence, an irreversible form of growth arrest [17,23]. Whereas inactivation of the senescence program allows progression of benign preneoplastic lesions to full-blown malignant cancers [24–27], its reactivation in murine tumors is associated with tumor regression [28,29]. To determine the state of senescence in tumors removed from DOX, we analyzed a panel of senescence-associated markers that we have found to be expressed in oncogenic C-RAF-induced lung tumors (Figure W3*B*). Similar to oncogenic K-*ras*–induced lung tumors, staining with antibodies against $p21^{Waf1}$, $p16^{INK4a}$, and HP-1γ revealed positive cells in tumors, whereas tumors removed from DOX were essentially negative (Figures W16*A* and W4*B*). Immunoblot analysis of lung tumor lysates confirmed the reduced expression of HP-1γ but not the $p21^{Waf1}$ and $p16^{INK4a}$ expressions that were absent in all samples presumably due to the low expression of these proteins (Figure W16*B*). In contrast to these senescence markers, p53 protein levels were found to be elevated during the tumor regression (Figure W16, *A* and *B*). Interestingly, the nuclear p53 expression that we detected in a small fraction of induced tumor cells switched to marked cytoplasmic staining during the tumor regression (Figure W16*A*).

Although cell cycle arrest was found to be part of tumor regression in many instances, complete elimination of tumors requires a cell death–related mechanism because cell cycle arrest will only induce a sustained tumor state. We therefore performed active (cleaved) caspase 3 immunostaining on lung tumor slides from DTR^{S} mice removed from the inducer. Surprisingly, we did not observe any positive cell after DOX withdrawal at any time point, indicating that tumors were not regressing through an apoptotic mechanism (Figure 4*D*). Similar results were obtained with TUNEL (Figure W17) or DNA fragmentation (Figure W18*A*) assays as well as by immunoblot analysis of tumor lysates with antibodies against cleaved caspase 3 or PARP cleavage (Figure W18*B*). Apart from apoptosis (type 1 cell death), autophagic (type 2 or macroautophagic) cell death, a process of self-degradation of cellular components, has often been proposed to be an alternative mechanism of programmed cell death. In contrast to apoptosis, autophagic cell death is caspase independent and does not involve classic DNA laddering. To address this possibility, we performed immunohistochemistry on lung tumor sections using microtubule-associated protein 1 light chain 3 (LC3) antibody that detects autophagosome formation [30]. In contrast to the control tumor sections, we detected very strong LC3 staining in all regressing lung tumors 1 or 2 weeks after DOX withdrawal (Figure 5, *A* and *B*). Punctuate pattern of LC3 staining rather than a cytosolic diffused pattern suggest the formation of autophagosomes typically formed during autophagy induction (Figure 5, *A* and *C*). Notably, consistent with lower autophagic capacity of cancer cell lines than their normal counterparts [31], we detected marked and diffused LC3 staining in nontumor region of the induced lung tumors (Figure W19). During autophagy, the LC3 cytosolic form (LC3-I) undergoes proteolytic cleavage and lipidation to generate the autophagic vacuole-bound and lipid-conjugated form (LC3-II) [32]. We therefore analyzed induction of LC3-I and its conversion to LC3-II, both being hallmarks of autophagy, in lung tumor samples by immunoblot analysis before and after DOX withdrawal. Consistent with strong LC3 expression in regressing tumors (Figure 5*A*), we found significantly increased LC3-I and LC3-II levels after deinduction indicating autophagy (Figure 5*D*). Analysis of other autophagy-related proteins such as Bcl-2 and Bcl-2–interacting protein, Beclin 1, did not show remarkable differences between the treatment groups (Figure 5*D*). To investigate the underlying mechanism of autophagy induction in our regressing lung tumors, we focused on mTOR signaling because this pathway was previously shown to play a role in autophagy suppression in several systems [33–35]. Toward this aim, components of the mTOR signaling were assessed in regressing lung tumor lysates by Western blot analysis. We found significantly decreased or no expression in all of the mTOR signaling–related markers that we have tested, except Raptor that is not expressed in all of the samples, after 1 week on removal of DOX (Figure 6*A*). Similarly, screening of lung tumor sections with phospho-specific (2448) mTOR antibody showed very strong reduction only in regressing lung tumors but not in their nonneoplastic regions such as bronchioles that were shown to be positive (Figure 6*B*).

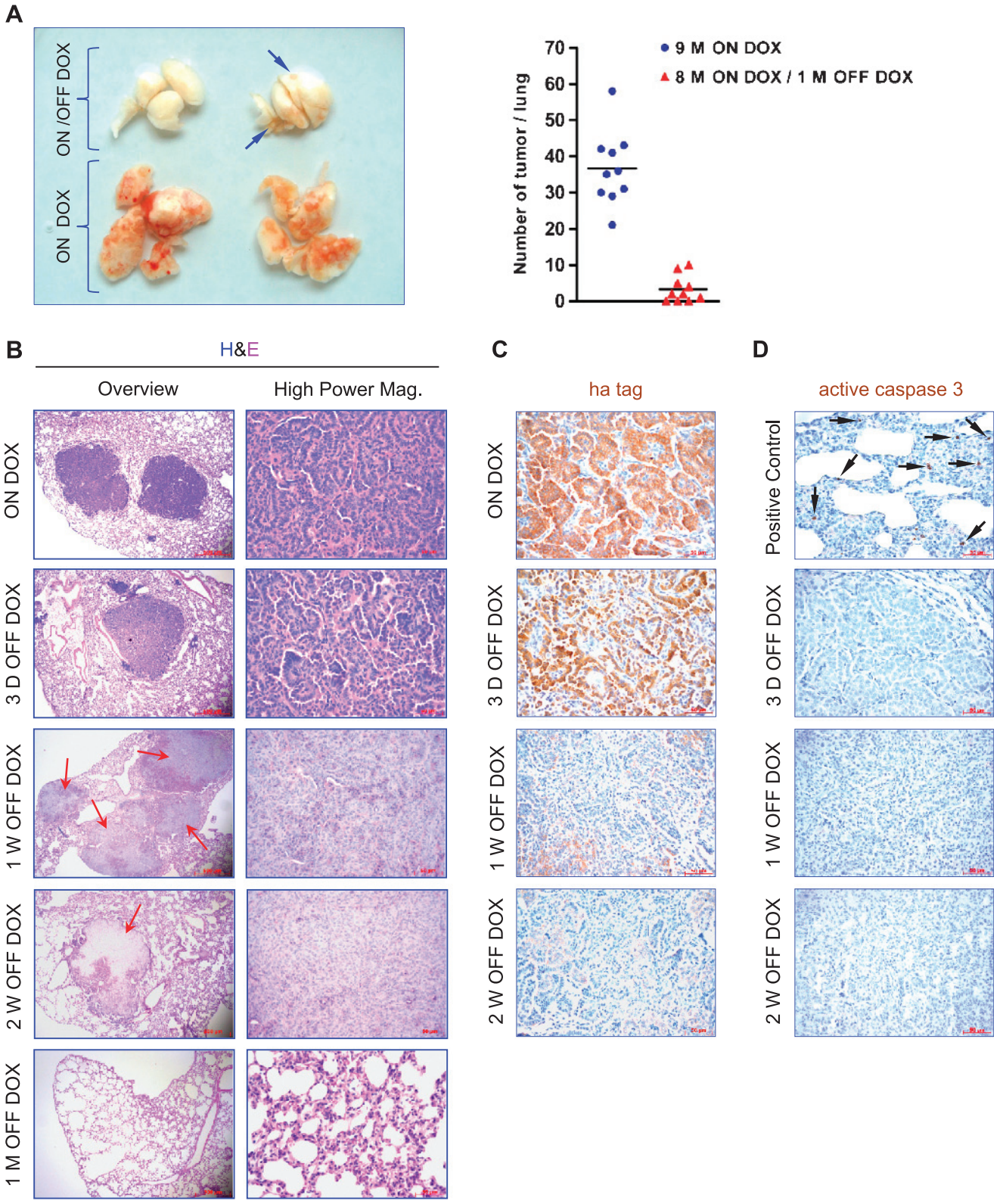

Figure 4. Oncogenic C-RAF expression is essential for lung tumor maintenance. (A) Inspection and quantitation of whole lungs from 8-month-induced DTR^S mice showing strong reduction in the tumor burden with few persistent nodules (arrows) after deinduction of oncogenic C-RAF for 1 month. The difference between the mice groups is statistically significant ($P < .05$), $n = 10$. (B) Representative examples of H&E-stained lung sections from the tumor-bearing DTR^S mice illustrating regressing tumor regions (red arrows) after DOX removal for the indicated time points. At least three mice were analyzed for each time point. (C and D) Staining of tumor-bearing lung sections with indicated markers before and after DOX withdrawal. For active caspase 3 immunostaining, a lung tumor section from DOX-treated *SP-C rtTA/Tet-O c-Myc* bitransgenic mice that we previously showed to induce apoptosis (arrowheads) [22] was used as a positive control. Hematoxylin (blue) was used as a counterstain.

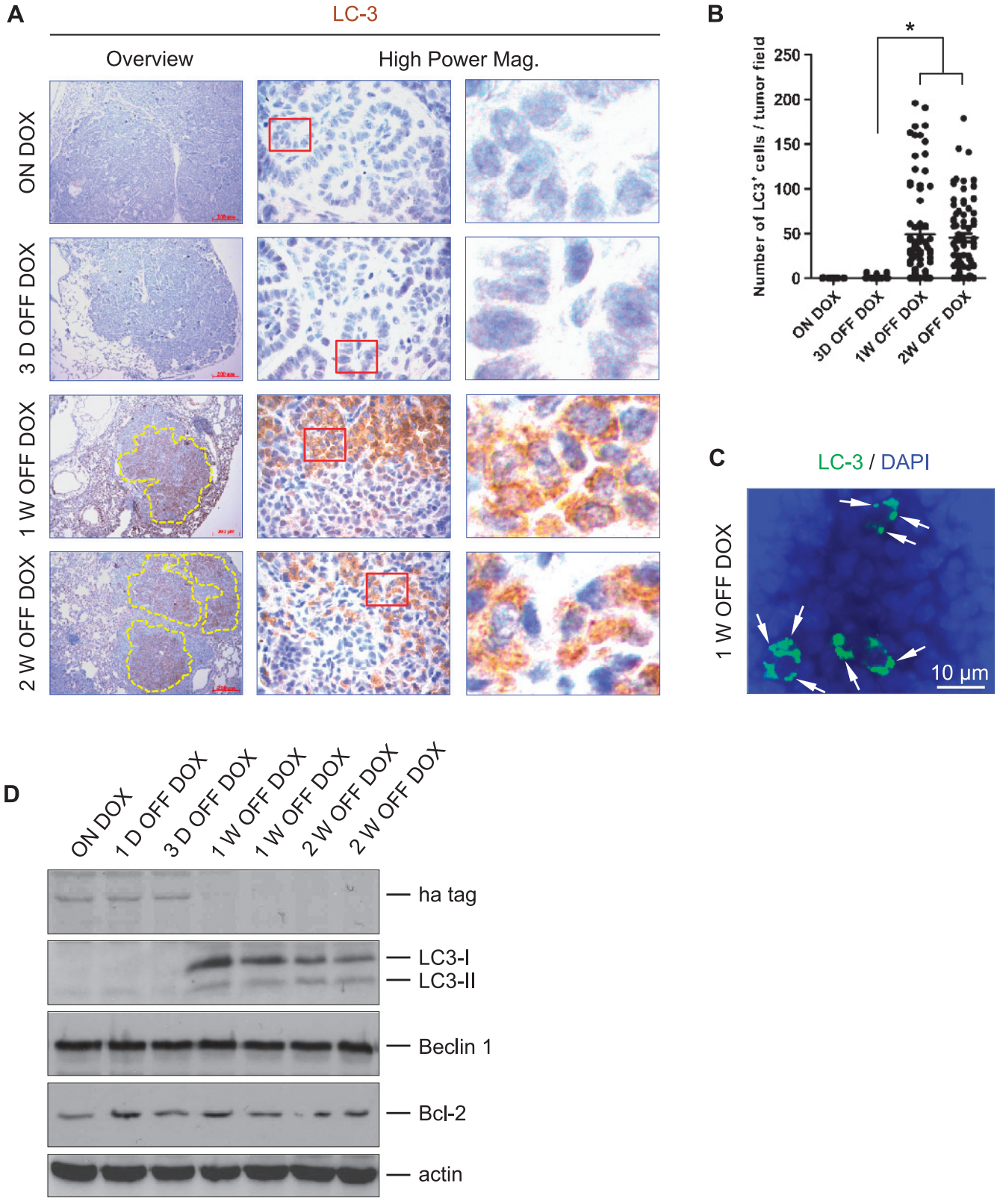

Figure 5. Tumor regression induced by DOX withdrawal is associated with autophagy. (A and B) Staining of lung sections from DTR^S mice with LC-3 antibody before and after DOX withdrawal. Circled areas (yellow) mark LC-3–positive (brown) regions. Hematoxylin (blue) was used as a counterstain. (B) Quantitation of LC-3 immunohistochemistry. At least 20 tumors from four mice for each time point of DOX treatment were assessed. *Statistically significant ($P < .05$). (C) Immunofluorescence staining of a regressing lung tumor section for LC-3 (green) showing a punctate staining pattern (arrows). Nuclei were counterstained with DAPI (blue). (D) Western blot analysis of lung tumor protein lysates from DTR^S mice with the indicated time points and markers.

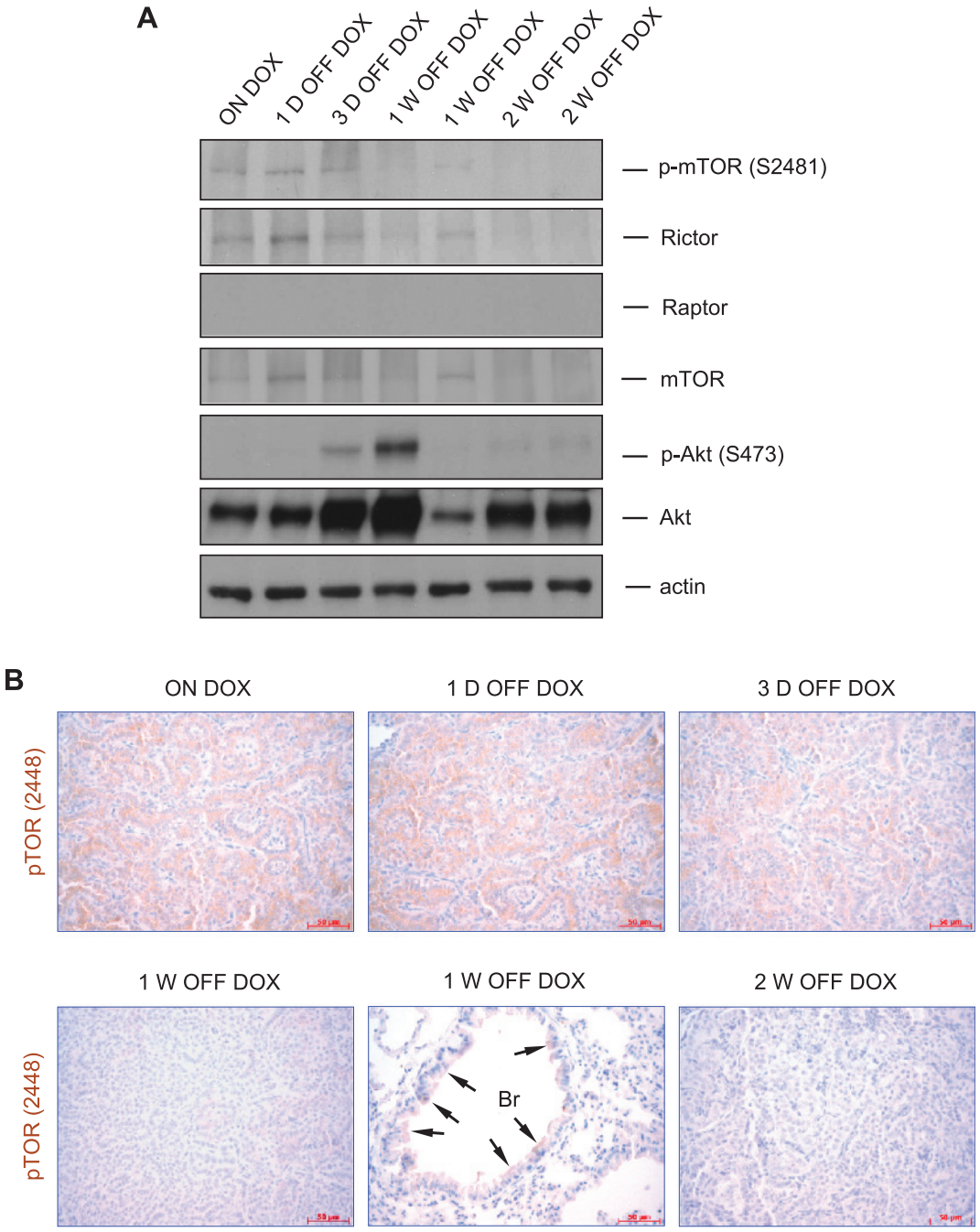

Figure 6. Down-regulation of mTOR signaling in regressing lung tumors. (A) Lung tumor lysates isolated at the indicated time points were immunoblotted with the indicated markers. (B) Immunohistochemistry of lung tumor sections with phospho-mTOR (2448)–specific antibody from the indicated DOX schedules. Arrows point out positive cells in a bronchiole (Br). Hematoxylin (blue) was used as a counterstain.

Inhibition of mTOR signaling and induction of autophagy judged by decreased phosphorylation of $p70^{S6K}$ and increased levels of LC3, respectively, in regressing lung tumor samples were associated with decreased levels of AMPKα phosphorylation, indicating that AMPK was not activated under these conditions (Figure W20).

Autophagy has also been associated with promotion of cell viability in several systems [36]. In line with this prosurvival role of autophagy, we observed a transient increase in phospho-Akt (Ser473) levels in tumors from mice recently removed from the inducer (Figure 6*A*). Taken together, these data demonstrate that deinduction of oncogenic C-RAF in established lung tumors triggers an autophagic cell death rather than apoptosis that ultimately leads to tumor shrinkage.

Discussion

Susceptibility of different cell types to oncogenic insults and oncogene addiction are important questions in tumor biology. Here we describe the generation and characterization of a new Tet-inducible oncogenic C-RAF transgenic mouse model for human NSCLC that sheds light on these questions. Our results reveal striking differences in

tumorigenicity between type II pneumocytes and bronchiolar Clara Cells, the cell types that are commonly believed to be the putative origin of human NSCLC [8]. Importantly, the present study establishes the first link between autophagic cell death and tumor regression.

A large body of earlier work has established that mutated components of the mitogenic cascade such as K-*ras*, B-RAF, and C-RAF are causally involved in the initiation and maintenance of lung neoplasia in mice [10,12,13,16,37–42]. Histopathologic examination of lung tumorigenesis in these animal models also highlighted major differences in tumor initiation, tumor numbers, tumor latency, as well as tumor cell morphology and tumor progression. Apart from their oncogenic actions, one possible explanation for these differences may be the distinct target cell specificities of the applied oncogenes. To test this hypothesis, we targeted oncogenic C-RAF expression to alveolar type II or bronchiolar Clara cells and evaluated tumor initiation and progression in the lung using a conditional transgenic system. The most striking outcome of this experiment was the failure of the lung tumor formation in most DTR^{C} mice compared with DTR^{S} mice. Intriguingly, rare lung tumors found in DTR^{C} mice did not seem to arise from Clara cells because these tumors both morphologically and histopathologically were indistinguishable from those found in DTR^{S} mice. It is therefore likely that these peripherally located rare lung tumors simply originated from type II cells rather than Clara cells as a result of ectopic expression of the rat *CCSP* promoter in mouse lung [19–21]. Whatever the tumor cell of origin is, the absence of lung adenomas in most DTR^{C} mice is in sharp contrast with the oncogenic K-ras^{G12C} mouse model in which multiple pulmonary tumors of type II cell lineage were formed when targeted by either *CCSP* or *SP-C* promoters [13]. The differential susceptibility of Clara cells or their precursor BASCs [43] to oncogenic–K-ras^{G12C} or –C-RAF might be related to their MAPK activation. Expression of oncogenic K-Ras results in a low to moderate activation of the MAPK pathway in the lung and leads to both alveolar and bronchiolar hyperplasias preceding the bronchiolocentric lung tumors [38,44]. As such, expression of C-RAF levels was found to be lower in tumors with *K-Ras* mutation than in those without mutation [45]. Oncogenic C-RAF, however, hyperactivates the MAPK pathway and predominantly forms alveolocentric tumors in the absence of preneoplastic lesions. If oncogenic C-RAF expression is targeted to either BASCs or Clara cells using *CCSP rtTA*, high MAPK activation might induce differentiation or transdifferentiation, respectively, toward the alveolar lineage. In this case, the *CCSP* promoter would be turned off and oncogenic C-RAF would no longer be expressed. Thus, transdifferentiation of Clara cells to alveolar type II cells as previously suggested [46] might be an underlying reason for loss of the oncogenic signal, preventing expansion of such tumor cells. Concomitant with CCSP loss, pro–SP-C expression that we found in bronchiolar hyperplasias from DTR^{C2} mice supports such a hypothesis. However, maintenance of the CCSP expression or absence of the bronchiolar hyperplasia in most DTR^{C2} mice suggests alternative mechanisms accounting for the resistance of BASC or Clara cells to neoplastic transformation induced by oncogenic C-RAF. Similar to C-RAF, oncogenic B-RAF also induces high activation of the MAPK pathway in the lung [13,16]. Interestingly, conditional expression of oncogenic B-RAF (V600E) using *CCSP rtTA* transgenic mice was shown to elicit multiple lung adenomas with alveolar type II cells features [13]. However, the authors performed these experiments only in the presence of *Ink4A*/*Arf*$^{-/-}$ background suggesting that additional genetic hits are required for the transformation of Clara cells by oncogenic C-RAF or B-RAF [13]. Recently, in a study of small cell lung carcinoma (SCLC), the susceptibility of lung lineage cells to oncogenic transformation by *Trp53* and *Rb1* inactivation was assessed. In this tumor model, similar to our results, Clara cells but not alveolar type II and neuroendocrine cells were found to be largely resistant to transformation [47] again suggesting a differential susceptibility of pulmonary epithelial cells to oncogenic insults.

One of the advantages of the conditional system that we used is the ability to turn off the transgene expression in established tumors and thus determine the role of oncogenes in tumor maintenance. Similar to other murine lung models, pulmonary tumors fueled by oncogenic C-RAF were also oncogene addicted because removal of transgene expression caused severe tumor regression. Earlier mouse lung tumor models in which oncogenic K-Ras (G12D or G12C) was conditionally expressed in pulmonary epithelial cells using *CCSP rtTA* mice showed conflicting results about the mechanism of tumor regression. Fisher et al. [12] showed that down-regulation of K-Ras^{G12D} in established lung tumors results in tumor shrinkage through apoptosis. In a similar bitransgenic mouse system where oncogenic K-Ras^{G12C} is the driver for lung tumorigenesis, Floyd et al. [42] showed that tumor regression was not occurring through apoptosis but rather through a mechanism alternative to apoptosis. In accordance with lack of apoptosis in CI-1040 (PD184352) MEK inhibitor–mediated tumor lung regression [48], we also did not detect apoptosis in oncogenic–C-RAF–driven lung tumors after DOX withdrawal. Tumor regression in the absence of apoptosis can also occur through reactivation of the cellular senescence program associated with differentiation and activation of innate immune response that targets tumor cells [28,29]. Consistent with oncogene-induced senescence, discontinuing oncogenic C-RAF expression from the established lung tumors led to a strong reduction in the senescence markers, indicating that the senescence program was not activated under this condition. Moreover, loss of differentiation and lack of inflammatory cells in lung tumors removed from the DOX suggest a different mechanism rather than senescence accounting for tumor shrinkage. Our further attempts to elucidate the mechanism of tumor clearance in our inducible system revealed induction of autophagy after down-regulation of oncogenic C-RAF. Apart from its role in cell death, autophagy ensures survival in nutrient-poor conditions through lysosomal recycling of intracellular nutrients [36]. Recent studies indicate that mTOR negatively controls autophagy as a downstream target for AKT/PKB in response to amino acids [49,50]. Such a negative regulation also exists in regressing lung tumors after shut down of oncogenic C-RAF. Currently, we do not know whether C-RAF directly regulates autophagy. Addiction of tumor cells to high levels of MAPK signaling rather than withdrawal of C-RAF expression may elicit cellular stress that leads to autophagy. The tumor suppressor p53 plays a critical role in sensing genotoxic and other stresses. Both activation and inhibition of autophagy were linked with p53, indicating a complex relationship between autophagy and p53 [51,52]. The mechanism by which p53 promotes autophagy was shown to be associated with DRAM transactivation [53] or mTOR inhibition through AMPK activation [51]. The negative regulation of mTOR by p53 was shown to be independent of the cell cycle regulation by p53 [51]. Elevated cytoplasmic p53 expression and inhibition of mTOR signaling in lung tumors discontinued from oncogenic C-RAF suggested p53/AMPK/mTOR signaling axis as an underlying mechanism; however, we found no evidence of AMPK activation under these conditions. The extent to which increased cytoplasmic p53 expression modulates autophagy induction in the present study remains to be determined.

In addition to RAF, oncogenic forms of RAS are also implicated in the negative control of autophagy, through activation of class I PI3K [54]. To check whether suppression of autophagy in C-RAF–induced lung tumors also involves activation of PI3-kinase signaling, we compared phospho-AKT (Ser473) levels, as a downstream component of PI3-kinase signaling. We observed an interesting phenomenon that the removal of the inducers from the already-established tumors caused a transient elevation of phospho-AKT (Ser473) that becomes undetectable after prolonged DOX withdrawal. Increased phospho-AKT (Ser473) levels in recently regressing lung tumors might have been resulted from the initial degradation of the cell organelles, which is then used for energy resources to enable cell survival. This observation might also be an example of dual function of autophagy in mediating both cell survival and cell death.

In summary, our results describe a novel mouse lung tumor model demonstrating differential tumorigenicity between pulmonary peripheral epithelial cells and providing a new tool for understanding oncogene addiction in the context of autophagy. We expect that these mice will be valuable in the future for the development of new anticancer therapeutics that specifically targets the RAS/RAF/MAPK pathways as well as in testing autophagy enhancers in the treatment of NSCLC.

Acknowledgments

The authors thank Jeffrey Whitsett for *SP-C rtTA* and *CCSP rtTA* mice and for the pro–SP-C antibody.

References

[1] Herbst RS, Heymach JV, and Lippman SM (2008). Lung cancer. *N Engl J Med* **359**, 1367–1380.

[2] Marks JL, McLellan MD, Zakowski MF, Lash AE, Kasai Y, Broderick S, Sarkaria IS, Pham D, Singh B, Miner TL, et al. (2007). Mutational analysis of EGFR and related signaling pathway genes in lung adenocarcinomas identifies a novel somatic kinase domain mutation in FGFR4. *PLoS One* **2**, e426.

[3] Rodenhuis S, Slebos RJ, Boot AJ, Evers SG, Mooi WJ, Wagenaar SS, van Bodegom PC, and Bos JL (1988). Incidence and possible clinical significance of K-*ras* oncogene activation in adenocarcinoma of the human lung. *Cancer Res* **48**, 5738–5741.

[4] Brose MS, Volpe P, Feldman M, Kumar M, Rishi I, Gerrero R, Einhorn E, Herlyn M, Minna J, Nicholson A, et al. (2002). *BRAF* and *RAS* mutations in human lung cancer and melanoma. *Cancer Res* **62**, 6997–7000.

[5] Naoki K, Chen TH, Richards WG, Sugarbaker DJ, and Meyerson M (2002). Missense mutations of the *BRAF* gene in human lung adenocarcinoma. *Cancer Res* **62**, 7001–7003.

[6] Cekanova M, Majidy M, Masi T, Al-Wadei HA, and Schuller HM (2007). Overexpressed Raf-1 and phosphorylated cyclic adenosine 3′-5′-monophosphate response element-binding protein are early markers for lung adenocarcinoma. *Cancer* **109**, 1164–1173.

[7] Blasco RB, Francoz S, Santamaria D, Canamero M, Dubus P, Charron J, Baccarini M, and Barbacid M (2011). c-Raf, but not B-Raf, is essential for development of K-*Ras* oncogene–driven non–small cell lung carcinoma. *Cancer Cell* **19**(5), 652–663.

[8] Meuwissen R and Berns A (2005). Mouse models for human lung cancer. *Genes Dev* **19**, 643–664.

[9] Palanisamy N, Ateeq B, Kalyana-Sundaram S, Pflueger D, Ramnarayanan K, Shankar S, Han B, Cao Q, Cao X, Suleman K, et al. (2010). Rearrangements of the RAF kinase pathway in prostate cancer, gastric cancer and melanoma. *Nat Med* **16**, 793–798.

[10] Kerkhoff E, Fedorov LM, Siefken R, Walter AO, Papadopoulos T, and Rapp UR (2000). Lung-targeted expression of the c-Raf-1 kinase in transgenic mice exposes a novel oncogenic character of the wild-type protein. *Cell Growth Differ* **11**, 185–190.

[11] Ceteci F, Ceteci S, Karreman C, Kramer BW, Asan E, Gotz R, and Rapp UR (2007). Disruption of tumor cell adhesion promotes angiogenic switch and progression to micrometastasis in RAF-driven murine lung cancer. *Cancer Cell* **12**, 145–159.

[12] Fisher GH, Wellen SL, Klimstra D, Lenczowski JM, Tichelaar JW, Lizak MJ, Whitsett JA, Koretsky A, and Varmus HE (2001). Induction and apoptotic regression of lung adenocarcinomas by regulation of a K-*Ras* transgene in the presence and absence of tumor suppressor genes. *Genes Dev* **15**, 3249–3262.

[13] Ji H, Wang Z, Perera SA, Li D, Liang MC, Zaghlul S, McNamara K, Chen L, Albert M, Sun Y, et al. (2007). Mutations in *BRAF* and *KRAS* converge on activation of the mitogen-activated protein kinase pathway in lung cancer mouse models. *Cancer Res* **67**, 4933–4939.

[14] Perl AK, Tichelaar JW, and Whitsett JA (2002). Conditional gene expression in the respiratory epithelium of the mouse. *Transgenic Res* **11**, 21–29.

[15] Degiulio JV, Kaufman CD, and Dean DA (2010). The SP-C promoter facilitates alveolar type II epithelial cell–specific plasmid nuclear import and gene expression. *Gene Ther* **17**, 541–549.

[16] Dankort D, Filenova E, Collado M, Serrano M, Jones K, and McMahon M (2007). A new mouse model to explore the initiation, progression, and therapy of $BRAF^{V600E}$-induced lung tumors. *Genes Dev* **21**, 379–384.

[17] Collado M, Gil J, Efeyan A, Guerra C, Schuhmacher AJ, Barradas M, Benguria A, Zaballos A, Flores JM, Barbacid M, et al. (2005). Tumour biology: senescence in premalignant tumours. *Nature* **436**, 642.

[18] Schramek D, Kotsinas A, Meixner A, Wada T, Elling U, Pospisilik JA, Neely GG, Zwick RH, Sigl V, Forni G, et al. (2011). The stress kinase MKK7 couples oncogenic stress to p53 stability and tumor suppression. *Nat Genet* **43**, 212–219.

[19] Stripp BR, Sawaya PL, Luse DS, Wikenheiser KA, Wert SE, Huffman JA, Lattier DL, Singh G, Katyal SL, and Whitsett JA (1992). *cis*-Acting elements that confer lung epithelial cell expression of the *CC10* gene. *J Biol Chem* **267**, 14703–14712.

[20] Tichelaar JW, Lu W, and Whitsett JA (2000). Conditional expression of fibroblast growth factor-7 in the developing and mature lung. *J Biol Chem* **275**, 11858–11864.

[21] Perl AK, Wert SE, Loudy DE, Shan Z, Blair PA, and Whitsett JA (2005). Conditional recombination reveals distinct subsets of epithelial cells in trachea, bronchi, and alveoli. *Am J Respir Cell Mol Biol* **33**, 455–462.

[22] Rapp UR, Korn C, Ceteci F, Karreman C, Luetkenhaus K, Serafin V, Zanucco E, Castro I, and Potapenko T (2009). *MYC* is a metastasis gene for non–small-cell lung cancer. *PLoS One* **4**, e6029.

[23] Collado M and Serrano M (2010). Senescence in tumours: evidence from mice and humans. *Nat Rev Cancer* **10**, 51–57.

[24] Braig M, Lee S, Loddenkemper C, Rudolph C, Peters AH, Schlegelberger B, Stein H, Dorken B, Jenuwein T, and Schmitt CA (2005). Oncogene-induced senescence as an initial barrier in lymphoma development. *Nature* **436**, 660–665.

[25] Chen Z, Trotman LC, Shaffer D, Lin HK, Dotan ZA, Niki M, Koutcher JA, Scher HI, Ludwig T, Gerald W, et al. (2005). Crucial role of p53-dependent cellular senescence in suppression of Pten-deficient tumorigenesis. *Nature* **436**, 725–730.

[26] Sarkisian CJ, Keister BA, Stairs DB, Boxer RB, Moody SE, and Chodosh LA (2007). Dose-dependent oncogene-induced senescence *in vivo* and its evasion during mammary tumorigenesis. *Nat Cell Biol* **9**, 493–505.

[27] Sun P, Yoshizuka N, New L, Moser BA, Li Y, Liao R, Xie C, Chen J, Deng Q, Yamout M, et al. (2007). *PRAK* is essential for *ras*-induced senescence and tumor suppression. *Cell* **128**, 295–308.

[28] Ventura A, Kirsch DG, McLaughlin ME, Tuveson DA, Grimm J, Lintault L, Newman J, Reczek EE, Weissleder R, and Jacks T (2007). Restoration of p53 function leads to tumour regression *in vivo*. *Nature* **445**, 661–665.

[29] Xue W, Zender L, Miething C, Dickins RA, Hernando E, Krizhanovsky V, Cordon-Cardo C, and Lowe SW (2007). Senescence and tumour clearance is triggered by p53 restoration in murine liver carcinomas. *Nature* **445**, 656–660.

[30] Tsuchihara K, Fujii S, and Esumi H (2009). Autophagy and cancer: dynamism of the metabolism of tumor cells and tissues. *Cancer Lett* **278**, 130–138.

[31] Gozuacik D and Kimchi A (2004). Autophagy as a cell death and tumor suppressor mechanism. *Oncogene* **23**, 2891–2906.

[32] Karim MR, Kanazawa T, Daigaku Y, Fujimura S, Miotto G, and Kadowaki M (2007). Cytosolic LC3 ratio as a sensitive index of macroautophagy in isolated rat hepatocytes and H4-II-E cells. *Autophagy* **3**, 553–560.

[33] Sudarsanam S and Johnson DE (2010). Functional consequences of mTOR inhibition. *Curr Opin Drug Discov Devel* **13**, 31–40.

[34] Jung CH, Ro SH, Cao J, Otto NM, and Kim DH (2010). mTOR regulation of autophagy. *FEBS Lett* **584**, 1287–1295.

[35] Chang YY, Juhasz G, Goraksha-Hicks P, Arsham AM, Mallin DR, Muller LK, and Neufeld TP (2009). Nutrient-dependent regulation of autophagy through the target of rapamycin pathway. *Biochem Soc Trans* **37**, 232–236.

[36] Debnath J, Baehrecke EH, and Kroemer G (2005). Does autophagy contribute to cell death? *Autophagy* **1**, 66–74.

[37] Johnson L, Mercer K, Greenbaum D, Bronson RT, Crowley D, Tuveson DA, and Jacks T (2001). Somatic activation of the K-*ras* oncogene causes early onset lung cancer in mice. *Nature* **410**, 1111–1116.

[38] Jackson EL, Willis N, Mercer K, Bronson RT, Crowley D, Montoya R, Jacks T, and Tuveson DA (2001). Analysis of lung tumor initiation and progression using conditional expression of oncogenic K-*ras*. *Genes Dev* **15**, 3243–3248.

[39] Meuwissen R, Linn SC, van der Valk M, Mooi WJ, and Berns A (2001). Mouse model for lung tumorigenesis through Cre/lox controlled sporadic activation of the K-*Ras* oncogene. *Oncogene* **20**, 6551–6558.

[40] Guerra C, Mijimolle N, Dhawahir A, Dubus P, Barradas M, Serrano M, Campuzano V, and Barbacid M (2003). Tumor induction by an endogenous K-*ras* oncogene is highly dependent on cellular context. *Cancer Cell* **4**, 111–120.

[41] Tuveson DA, Shaw AT, Willis NA, Silver DP, Jackson EL, Chang S, Mercer KL, Grochow R, Hock H, Crowley D, et al. (2004). Endogenous oncogenic K-*ras*(G12D) stimulates proliferation and widespread neoplastic and developmental defects. *Cancer Cell* **5**, 375–387.

[42] Floyd HS, Farnsworth CL, Kock ND, Mizesko MC, Little JL, Dance ST, Everitt J, Tichelaar J, Whitsett JA, and Miller MS (2005). Conditional expression of the mutant Ki-ras^{G12C} allele results in formation of benign lung adenomas: development of a novel mouse lung tumor model. *Carcinogenesis* **26**, 2196–2206.

[43] Kim CF, Jackson EL, Woolfenden AE, Lawrence S, Babar I, Vogel S, Crowley D, Bronson RT, and Jacks T (2005). Identification of bronchioalveolar stem cells in normal lung and lung cancer. *Cell* **121**, 823–835.

[44] Sweet-Cordero A, Tseng GC, You H, Douglass M, Huey B, Albertson D, and Jacks T (2006). Comparison of gene expression and DNA copy number changes in a murine model of lung cancer. *Genes Chromosomes Cancer* **45**, 338–348.

[45] Ramakrishna G, Bialkowska A, Perella C, Birely L, Fornwald LW, Diwan BA, Shiao YH, and Anderson LM (2000). Ki-*ras* and the characteristics of mouse lung tumors. *Mol Carcinog* **28**, 156–167.

[46] Ten Have-Opbroek AA, Benfield JR, van Krieken JH, and Dijkman JH (1997). The alveolar type II cell is a pluripotential stem cell in the genesis of human adenocarcinomas and squamous cell carcinomas. *Histol Histopathol* **12**, 319–336.

[47] Sutherland KD, Proost N, Brouns I, Adriaensen D, Song JY, and Berns A (2011). Cell of origin of small cell lung cancer: inactivation of Trp53 and Rb1 in distinct cell types of adult mouse lung. *Cancer Cell* **19**, 754–764.

[48] Kramer BW, Gotz R, and Rapp UR (2004). Use of mitogenic cascade blockers for treatment of C-Raf induced lung adenoma *in vivo*: CI-1040 strongly reduces growth and improves lung structure. *BMC Cancer* **4**, 24.

[49] van Sluijters DA, Dubbelhuis PF, Blommaart EF, and Meijer AJ (2000). Amino-acid–dependent signal transduction. *Biochem J* **351**(Pt 3), 545–550.

[50] Oldham S and Hafen E (2003). Insulin/IGF and target of rapamycin signaling: a TOR de force in growth control. *Trends Cell Biol* **13**, 79–85.

[51] Feng Z, Zhang H, Levine AJ, and Jin S (2005). The coordinate regulation of the p53 and mTOR pathways in cells. *Proc Natl Acad Sci USA* **102**, 8204–8209.

[52] Tasdemir E, Maiuri MC, Galluzzi L, Vitale I, Djavaheri-Mergny M, D'Amelio M, Criollo A, Morselli E, Zhu C, Harper F, et al. (2008). Regulation of autophagy by cytoplasmic p53. *Nat Cell Biol* **10**, 676–687.

[53] Crighton D, Wilkinson S, O'Prey J, Syed N, Smith P, Harrison PR, Gasco M, Garrone O, Crook T, and Ryan KM (2006). DRAM, a p53-induced modulator of autophagy, is critical for apoptosis. *Cell* **126**, 121–134.

[54] Furuta S, Hidaka E, Ogata A, Yokota S, and Kamata T (2004). Ras is involved in the negative control of autophagy through the class I PI3-kinase. *Oncogene* **23**, 3898–3904.

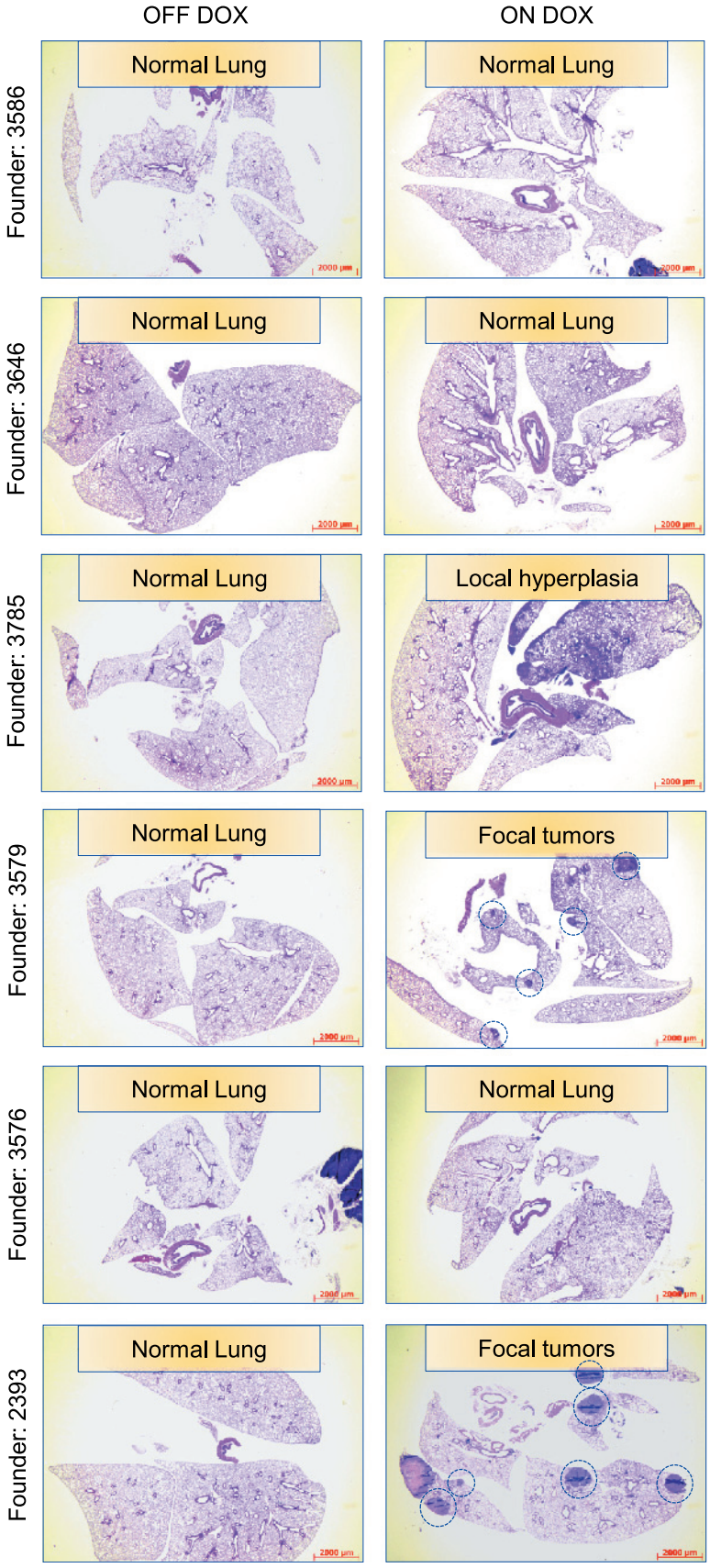

Figure W1. Analysis of lung tumor induction in different Tet-O C-RAF ha-BxB transgenic mouse founders. Each responder founder line was crossed with *SP-C rtTA* inducer line to generate double-transgenic (DTR) mice. Representative pictures of H&E-stained lung sections from DTR mice before and after DOX administration. Blue circles indicate focal pulmonary tumors.

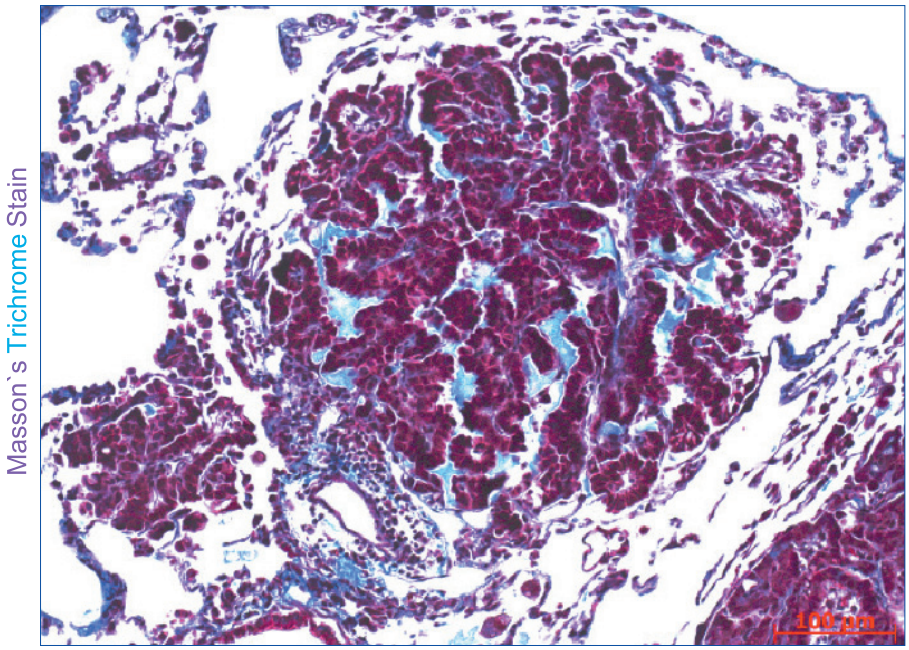

Figure W2. Collagen expression in oncogenic C-RAF–driven lung tumors. Masson trichrome staining of a representative lung tumor section from a 9-month-induced DTR^{S} mouse showing collagen expression (blue).

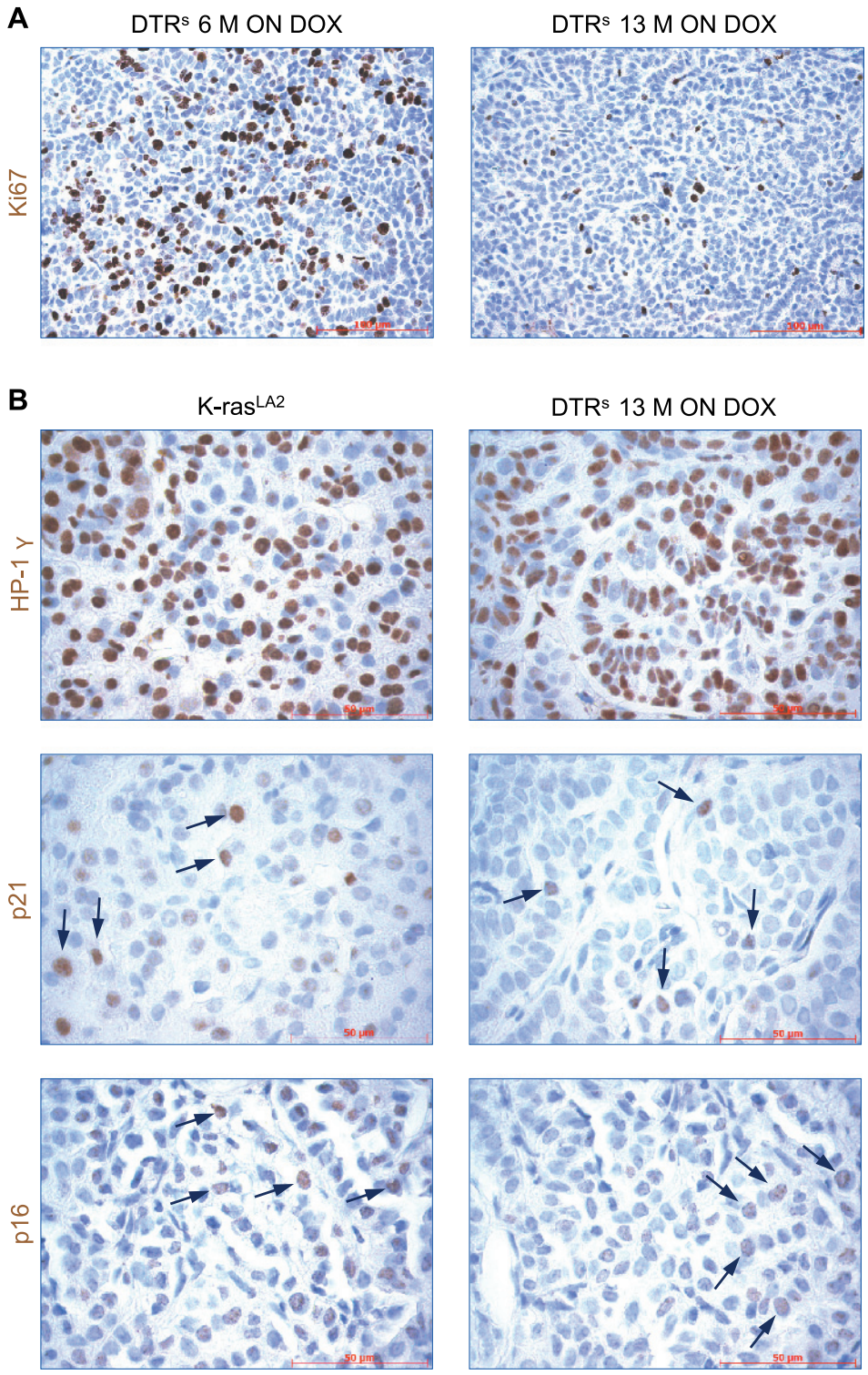

Figure W3. Lung tumors induced by oncogenic C-RAF are positive for the markers of senescence. (A) Ki67 staining (brown) of lung tumor sections from induced DTR^{S} mice showing diminished proliferation after prolonged induction. (B) Immunohistochemical analysis of sections from K-*ras*^{LA2}– or oncogenic C-RAF–induced lung tumors for the indicated antibodies. Arrows indicate positive cells for the corresponding protein. Hematoxylin (blue) was used as a counterstain for immunohistochemistry.

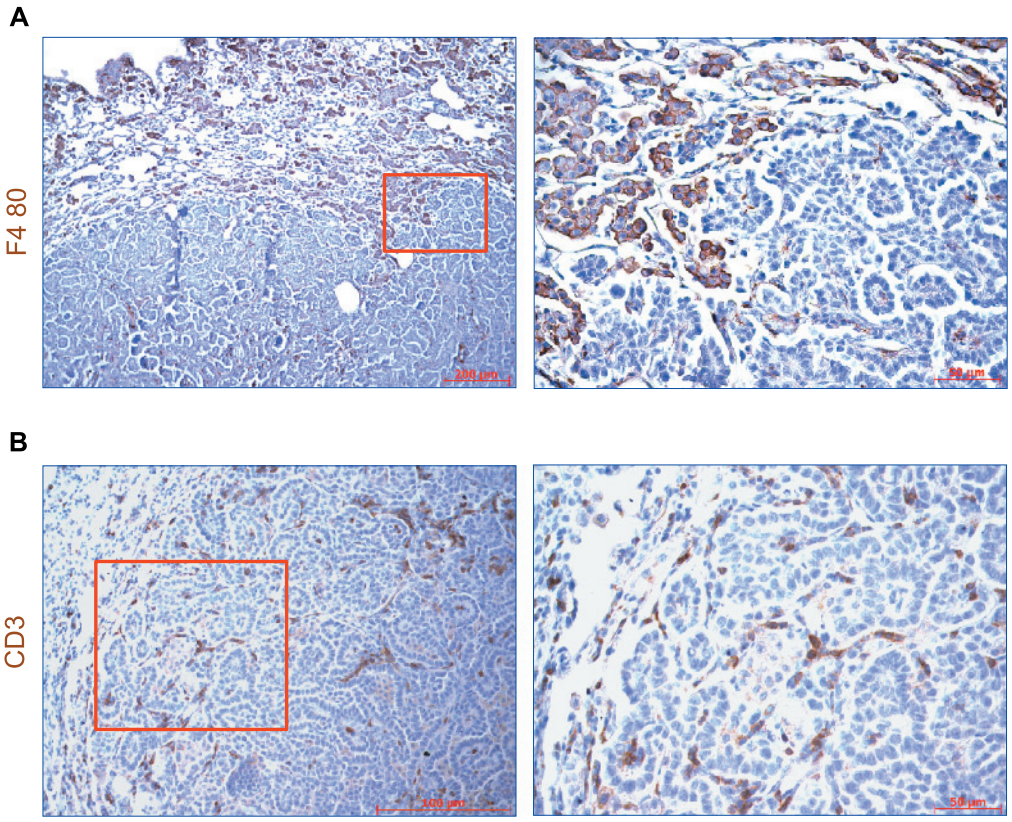

Figure W4. Analysis of immune cells in oncogenic C-RAF–driven lung tumors. (A and B) Immunohistochemistry of lung tumor sections for immune cells markers as indicated. Right panel pictures are the higher magnifications of the insets. Hematoxylin (blue) was used as a counterstain for immunohistochemistry.

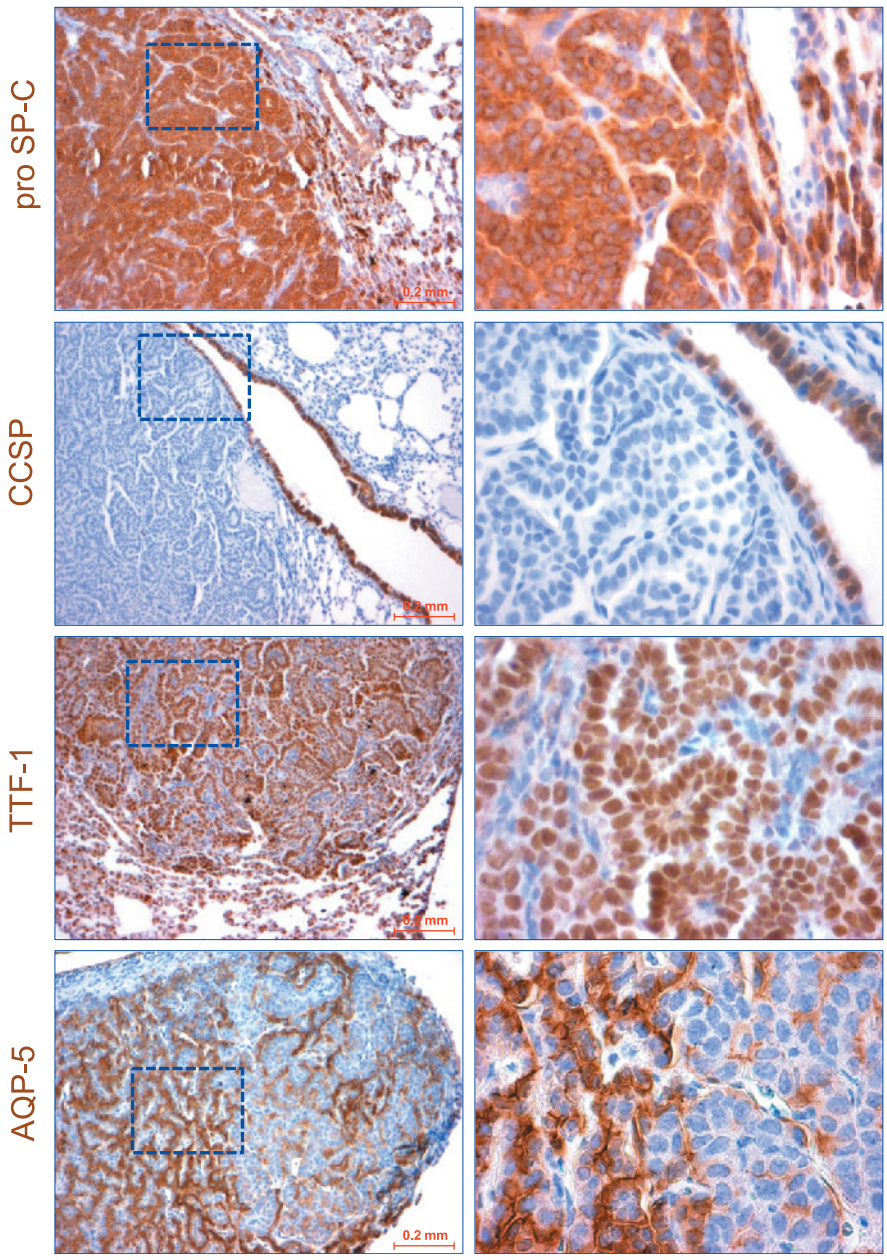

Figure W5. Assessment of lung lineage markers in induced tumors. Lung sections (fixed in formalin) from induced (12 months) DTR^{S} mice were immunostained with the indicated antibodies. Higher-magnification views of the boxed tumor regions are shown in the right panels. As a counterstain, hematoxylin (blue) was used.

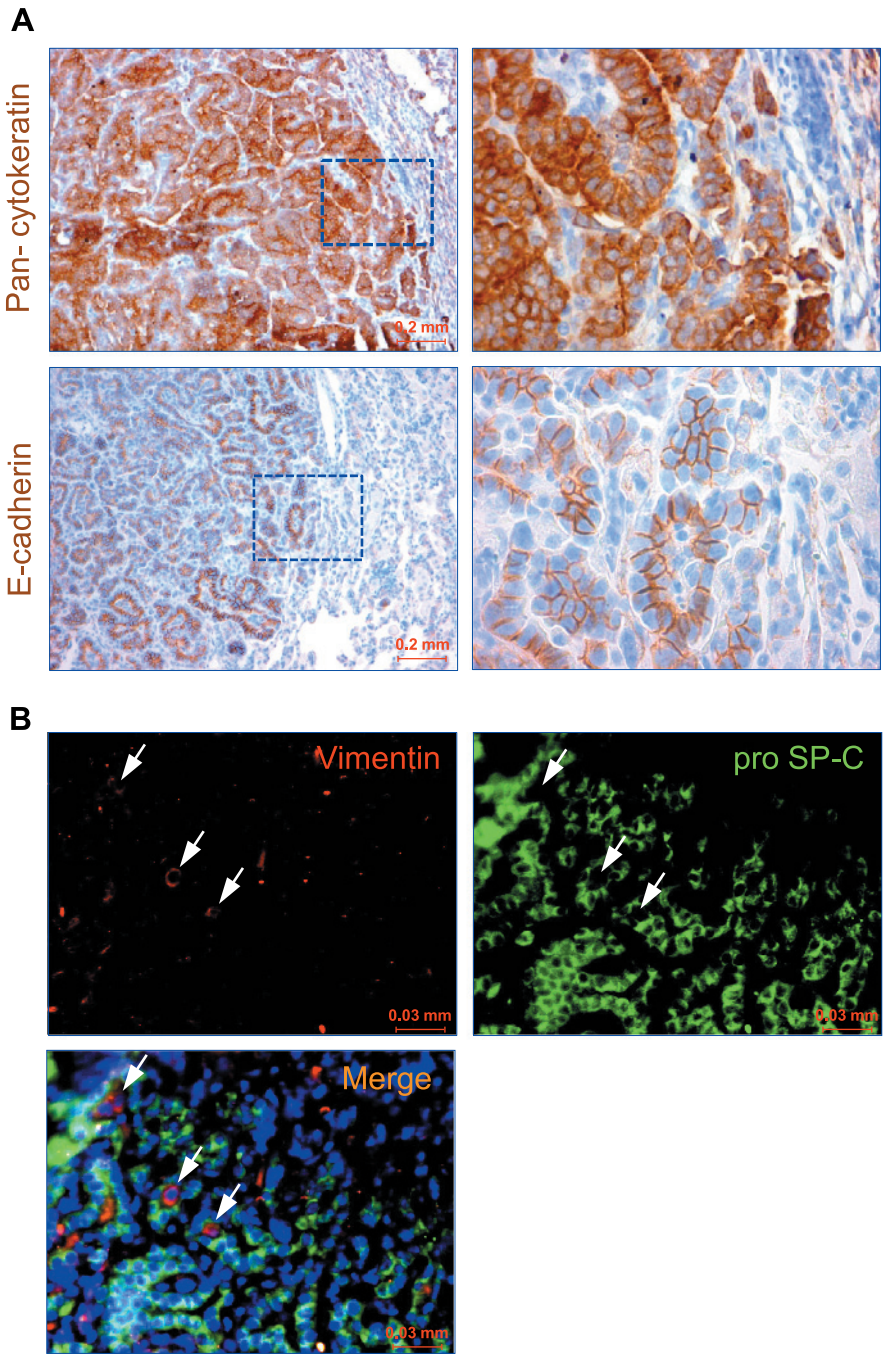

Figure W6. Evaluation of EMT markers in induced lung tumors from DTR^{S} mice. (A) Immunohistochemistry for paraffin-embedded lung sections from 15-month-induced DTR^{S} mice with the indicated antibodies; right panel pictures are the higher-magnification views of the boxed areas (blue). (B) Immunofluorescence costaining of lung sections with the indicated antibodies. Tumor cells were marked by pro–SP-C (green) expression. Arrows point out rare vimentin-positive (red) cells that are negative for pro–SP-C (merge). DAPI (blue) shows nuclei.

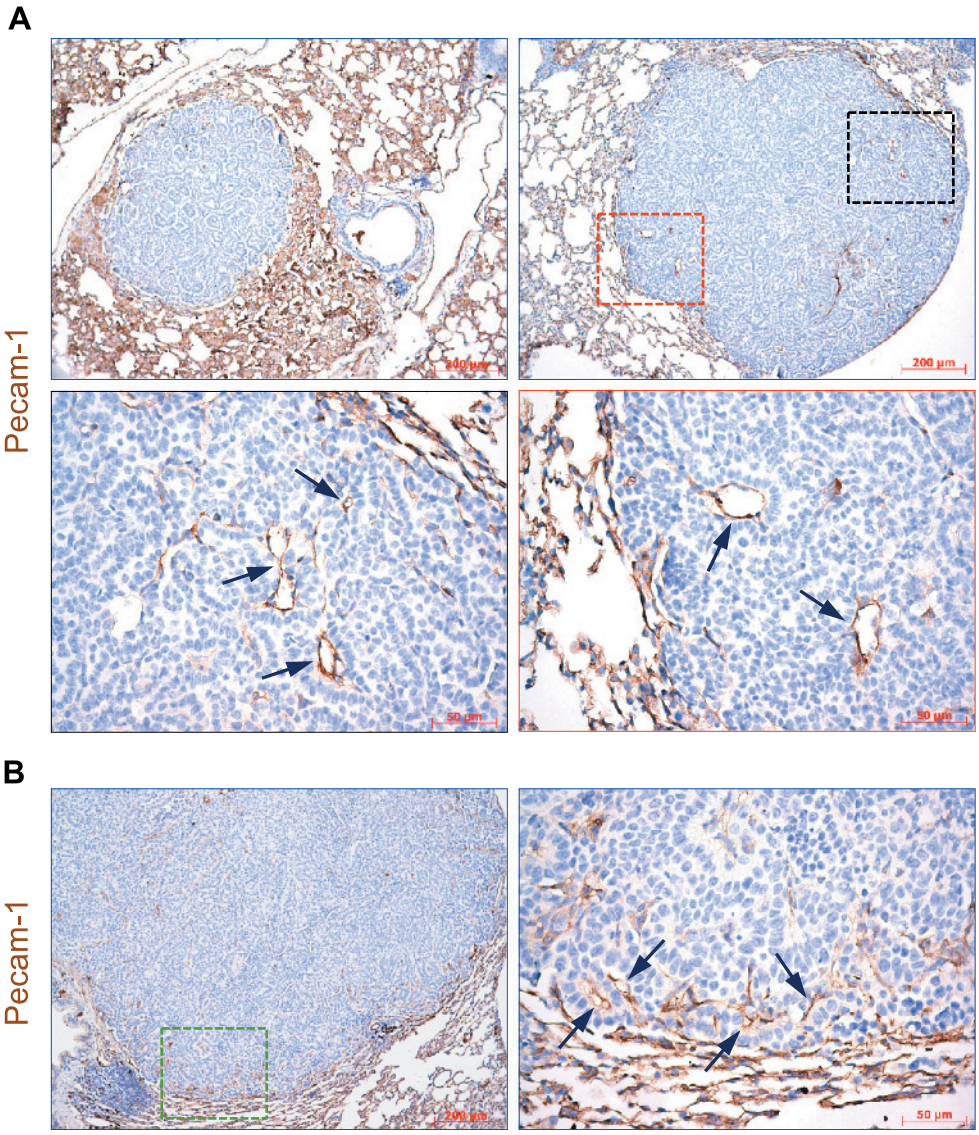

Figure W7. Lack of angiogenic switch induction in macroscopic pulmonary tumors fueled by oncogenic C-RAF. (A) Lung tumor sections from 6- (top left) and 9-month- (top right) induced DTR^S mice were stained with Pecam-1 antibody for evaluation of tumor vasculature. Pictures shown at the bottom (left and right) are the higher-magnification views of the black and red boxed areas, respectively. Blue arrows demonstrate peritumoral blood vessels. (B) Representative Pecam-1 immunohistochemistry of a tumor lung section obtained from a long-term (17 months) DOX-treated DTR^S mouse. Image on the right side represents a higher-magnification view of the area indicated by the green box. Arrows (blue) point out peritumoral blood vessels. Hematoxylin (blue) was used for counterstaining.

Age: 2 - 8 months ; n= 19					
Tissues	Lymph Node	Liver	Brain	Pancreas	Kidney
Metastasis	0 / 19	0 / 19	0 / 19	0 / 19	0 / 19
Age: 8 - 18 months ; n= 26					
Tissues	Lymph Node	Liver	Brain	Pancreas	Kidney
Metastasis	0 / 26	0 / 26	0 / 26	0 / 26	0 / 26

Figure W8. Incidence of metastasis. Paraffin-embedded sections of indicated organs obtained from young and old-aged cohorts of DTR^S mice were screened for regional and distant colonization of tumor cells by immunohistochemistry using antibodies against Pan-cytokeratin and ha-tag. LN indicates lymph node (include mediastinal and axillary lymph nodes). Animal numbers (*n*) and ages are as indicated.

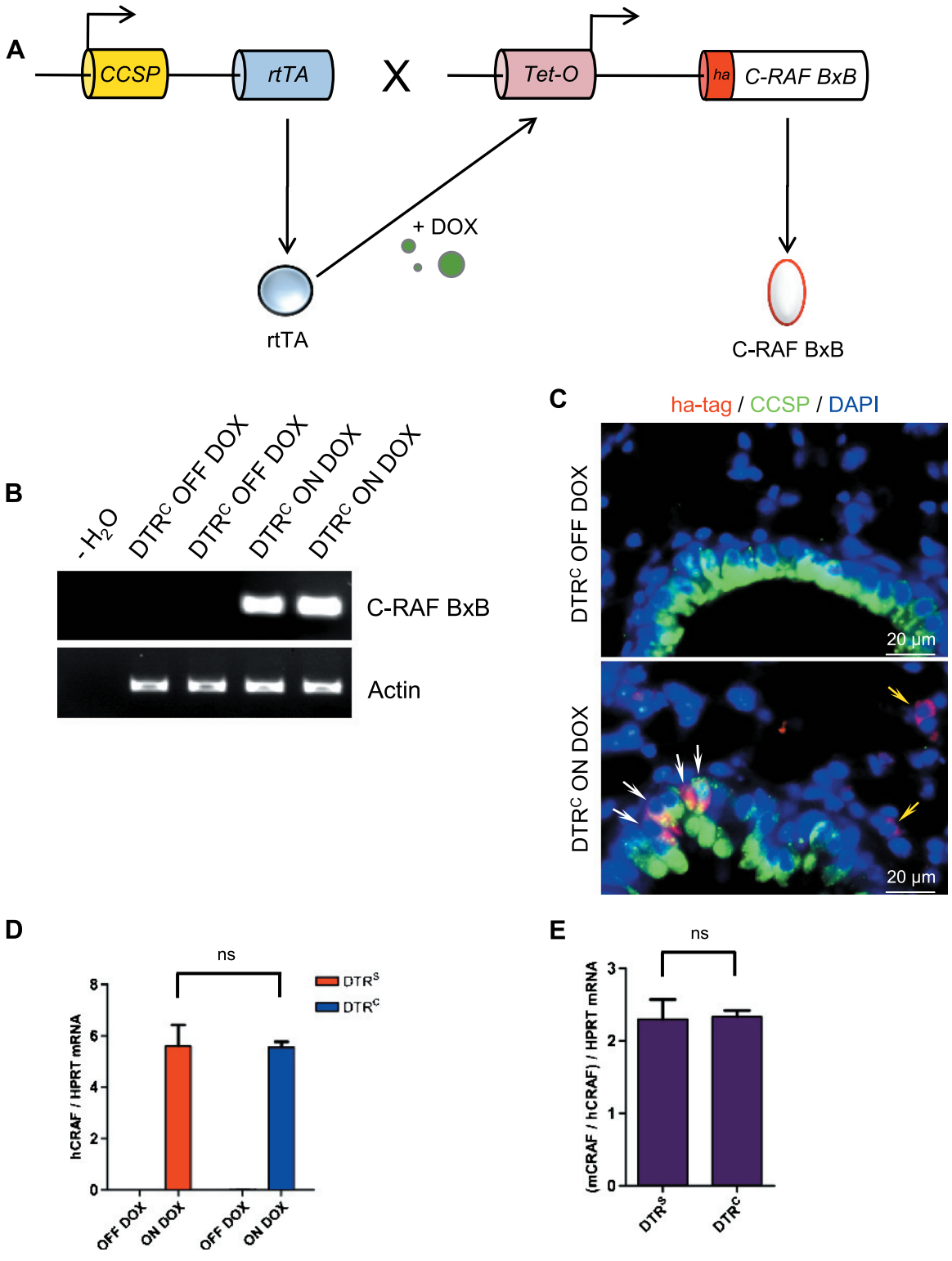

Figure W9. Targeting and analysis of oncogenic C-RAF expression in bronchiolar Clara cells using *CCSP rtTA* mice. (A) Schematic representation of the constructs for conditional expression of oncogenic C-RAF in Clara cell lineage. (B) RT-PCR analysis of total lung samples prepared from DTR^C mice demonstrates oncogenic C-RAF (C-RAF BxB) transcript only in induced mice. The transcript of β-actin serves as an internal control. (C) Dual immunofluorescence staining of paraffin-embedded lung sections from DTR^C mice with CCSP and ha-tag antibodies showing oncogenic C-RAF expression in bronchiolar epithelial cells (white arrows) and in a subset of alveolar epithelial cells (yellow arrows) after DOX treatment. DAPI (blue) shows nuclei. (D and E) Real-time RT-PCR analysis of oncogenic C-RAF (hCRAF) and its comparison to endogenous expression of C-RAF (mCRAF) between DTR^S and DTR^C mice. h indicates human; m, mouse. Error bars are SEM from four different mice for each category. ns indicates not significant.

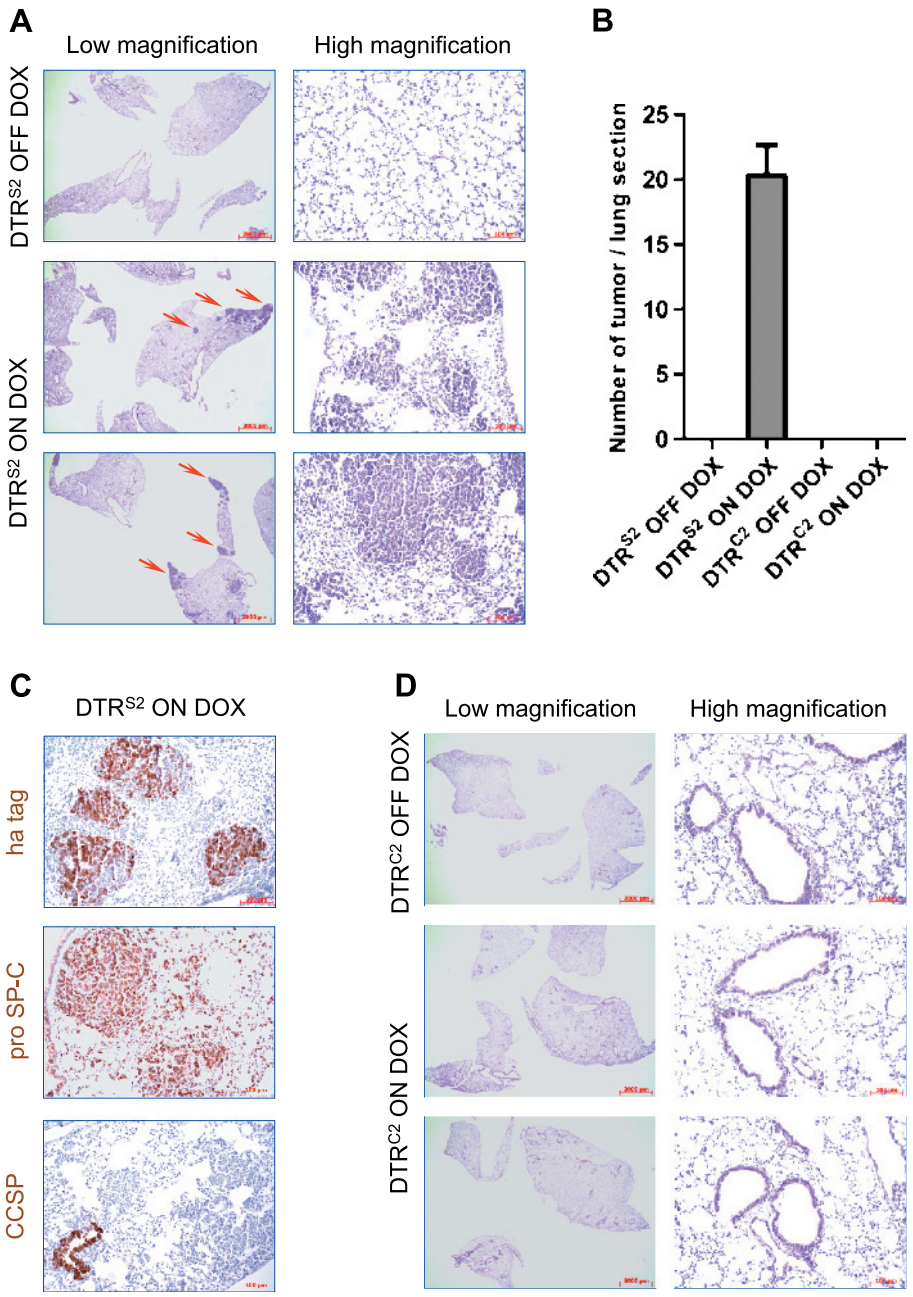

Figure W10. Comparison of lung tumor induction potential between DTR^{S2} and DTR^{C2} mice using Tet-O C-RAF ha-BxB 3579 founder line. (A) Representative pictures of H&E-stained lung sections from control (OFF DOX) and embryonically induced (ON DOX) DTR^{S2} mice. Red arrows point out pulmonary lung adenomas. (B) Quantitation of tumor load between the groups as indicated. Error bars are SEM from six different mice for each category. (C) Staining of lung tumor sections from DTR^{S2} mice with the indicated markers. Hematoxylin (blue) was used as a counterstain. (D) H&E-stained lung sections from control and induced DTR^{C2} mice showing the absence of pulmonary tumors or bronchiolar hyperplasia.

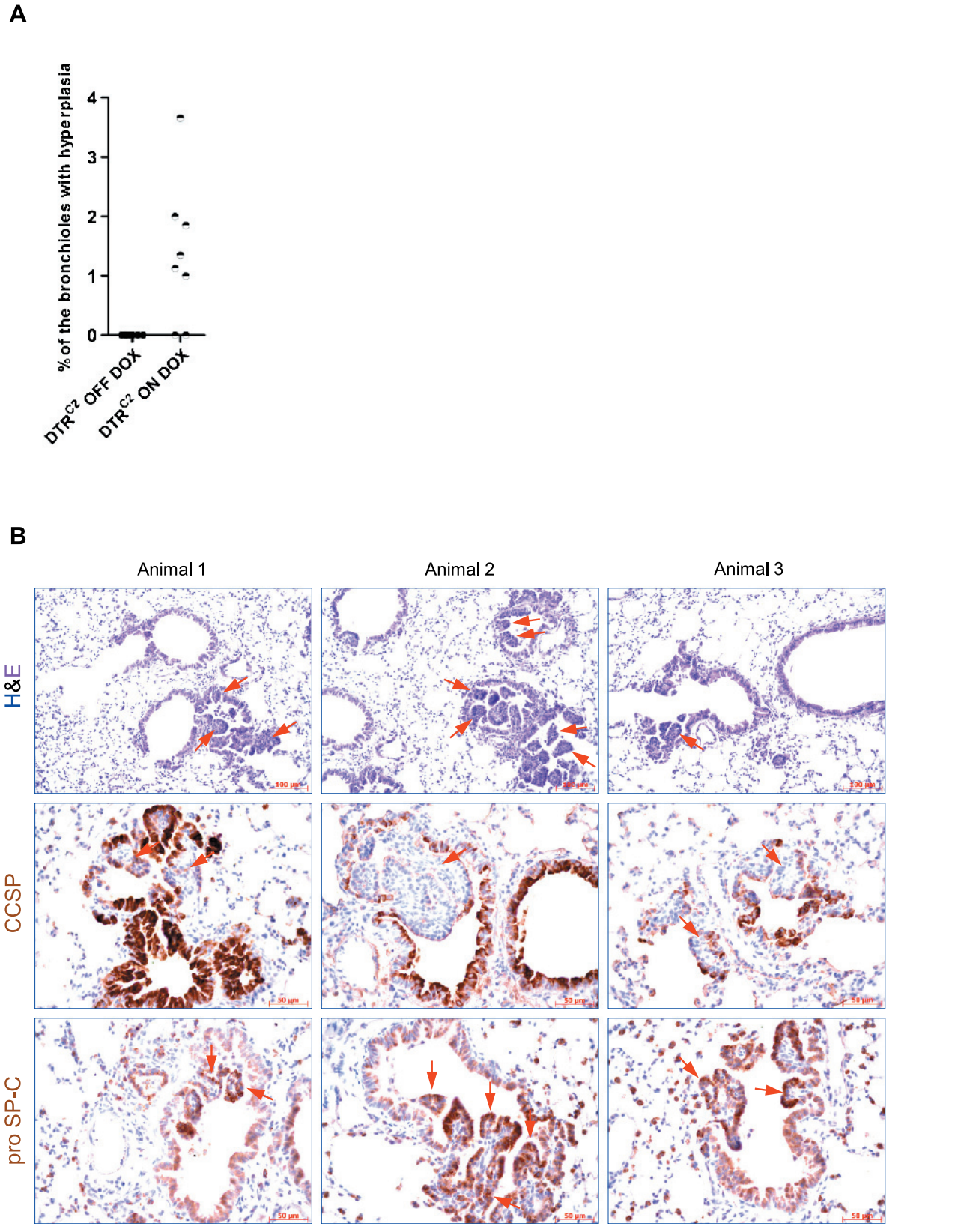

Figure W11. Formation of bronchiolar hyperplasia and their transdifferentiation to alveolar lineage in induced DTR^{C2} mice. (A) Incidence of bronchiolar hyperplasia. At least 450 terminal bronchioles were evaluated from lung sections of eight mice for each group. (B) Staining of lung sections from different animals carrying bronchiolar hyperplasia with the indicated markers. Red arrows points out papillary epithelial hyperplasias.

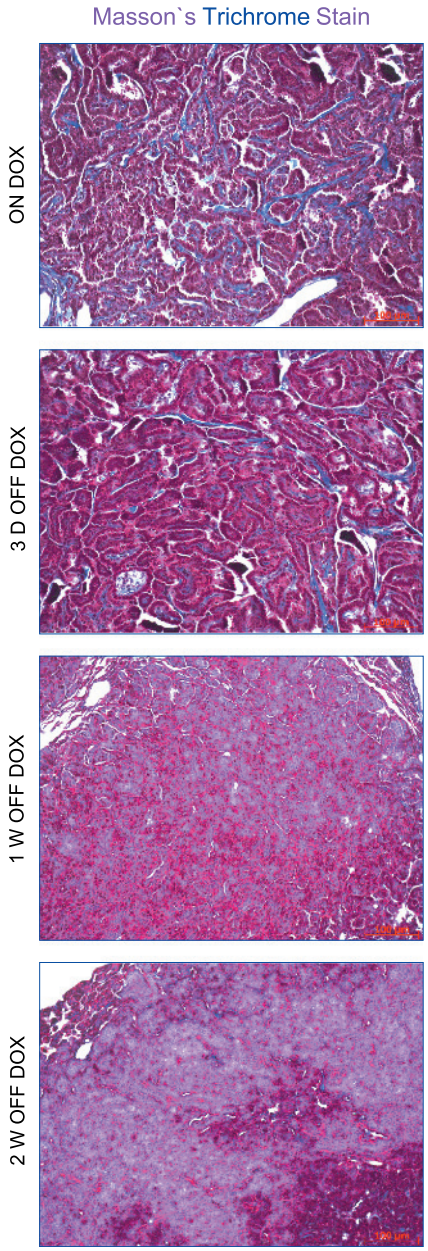

Figure W12. Loss of collagen expression in regressing lung tumors. Masson trichrome staining of lung tumor sections from DTR^S mice showing strong reduction in collagen expression (blue) after DOX removal at the indicated time points.

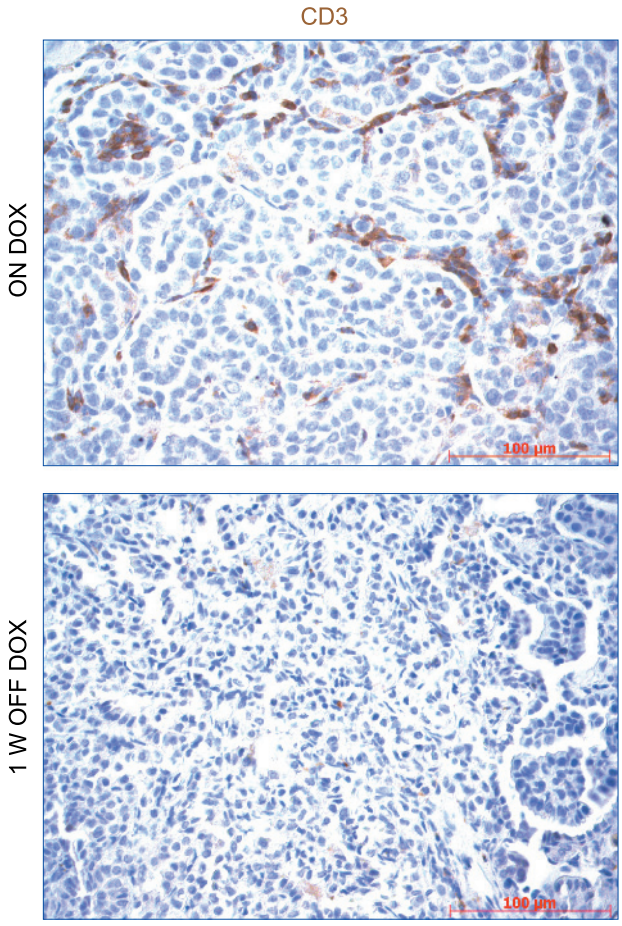

Figure W13. Absence of T cells in regressing lung tumors. Immunohistochemistry of lung tumor sections from DTR^S mice for CD3 antibody showing disappearance of T cells after 1 week of DOX withdrawal. Hematoxylin (blue) was used as a counterstain for immunohistochemistry.

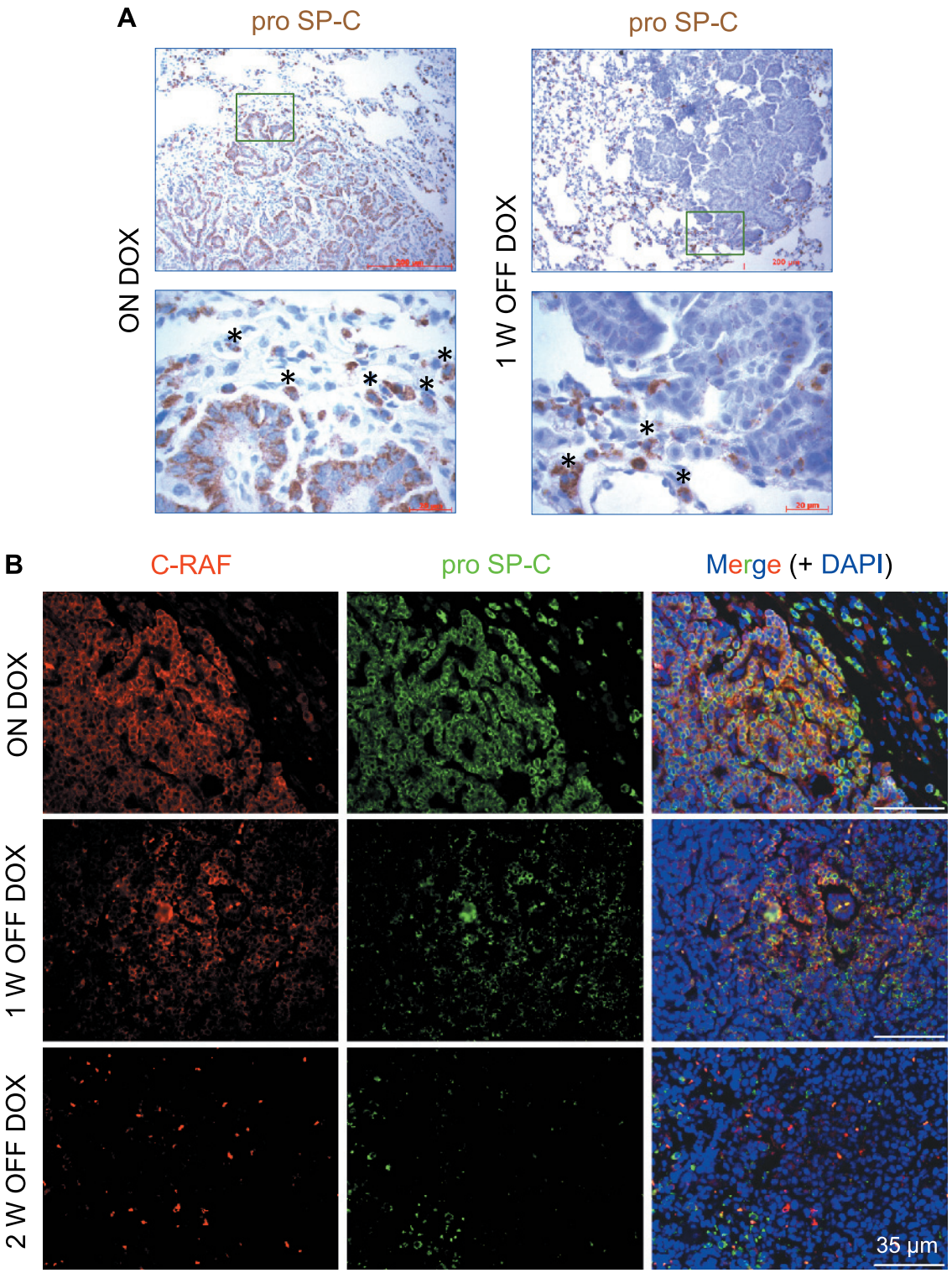

Figure W14. Loss of cell differentiation during tumor regression. (A) Immunohistochemistry of lung tumor sections from DTR^S mice with pro–SP-C antibody showing loss of differentiation after DOX removal. Pictures shown at the bottom are the higher-magnification views of the insets. Asterisks mark pro–SP-C–expressing alveolar type II cells. Hematoxylin (blue) was used as a counterstain for immunohistochemistry. (B) Dual immunofluorescence staining of the lung tumor sections for indicated markers confirming the upper results. Nuclei were counterstained with DAPI (blue).

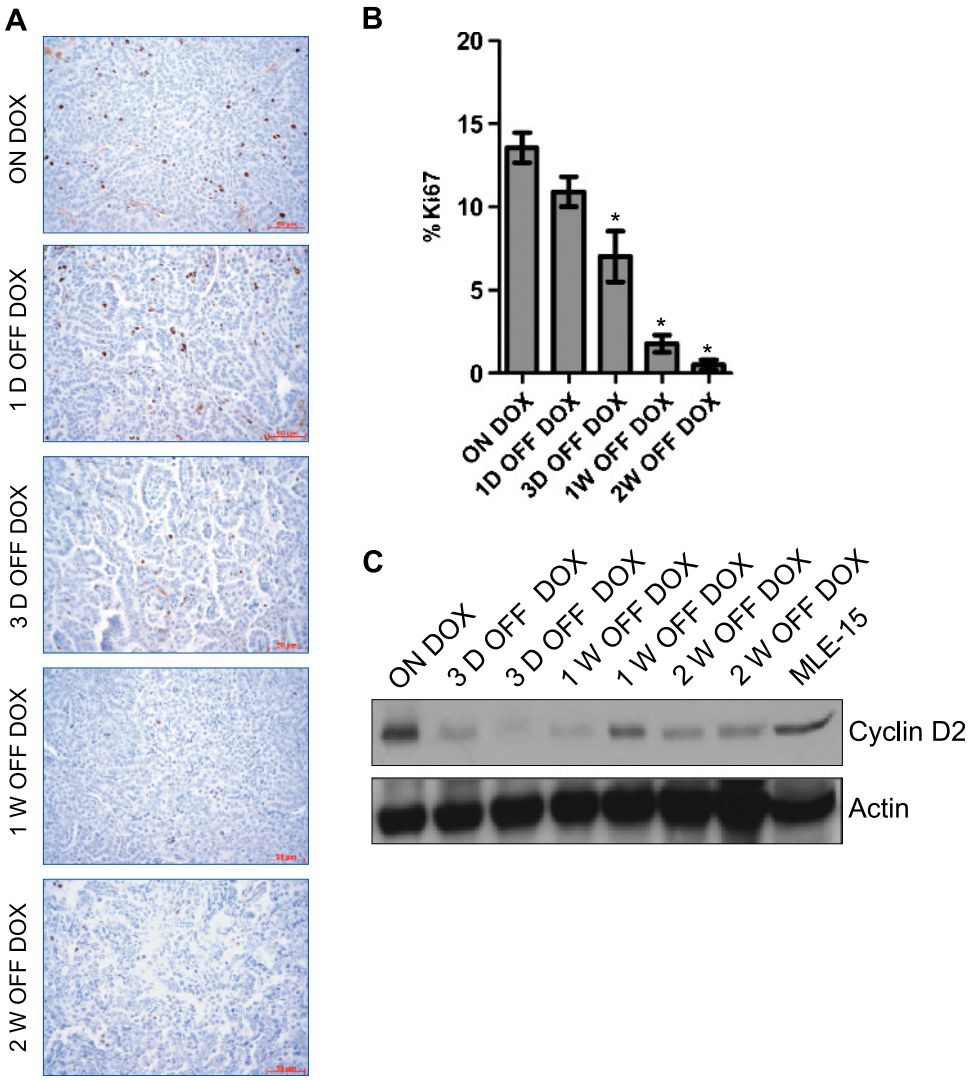

Figure W15. Down-regulation of oncogenic C-RAF by DOX withdrawal in induced lung tumors leads to cell cycle arrest. (A) Sections of lungs from DTR^S mice treated with DOX for 8 months and after removal of the inducer for 1 day, 3 days, 1 week, or 2 weeks were immunostained for Ki67 (brown). Hematoxylin (blue) was used as a counterstain for immunohistochemistry. (B) Quantitation of Ki67 immunohistochemistry. At least 10 different random tumor areas were counted for each mouse. Error bars are SEM from four different mice for each category. *Statistically significant ($P < .05$). (C) Immunoblot analysis of lung tumor protein lysates from induced or DOX-removed DTR^S mice for cyclin D2. Actin was used as a loading control.

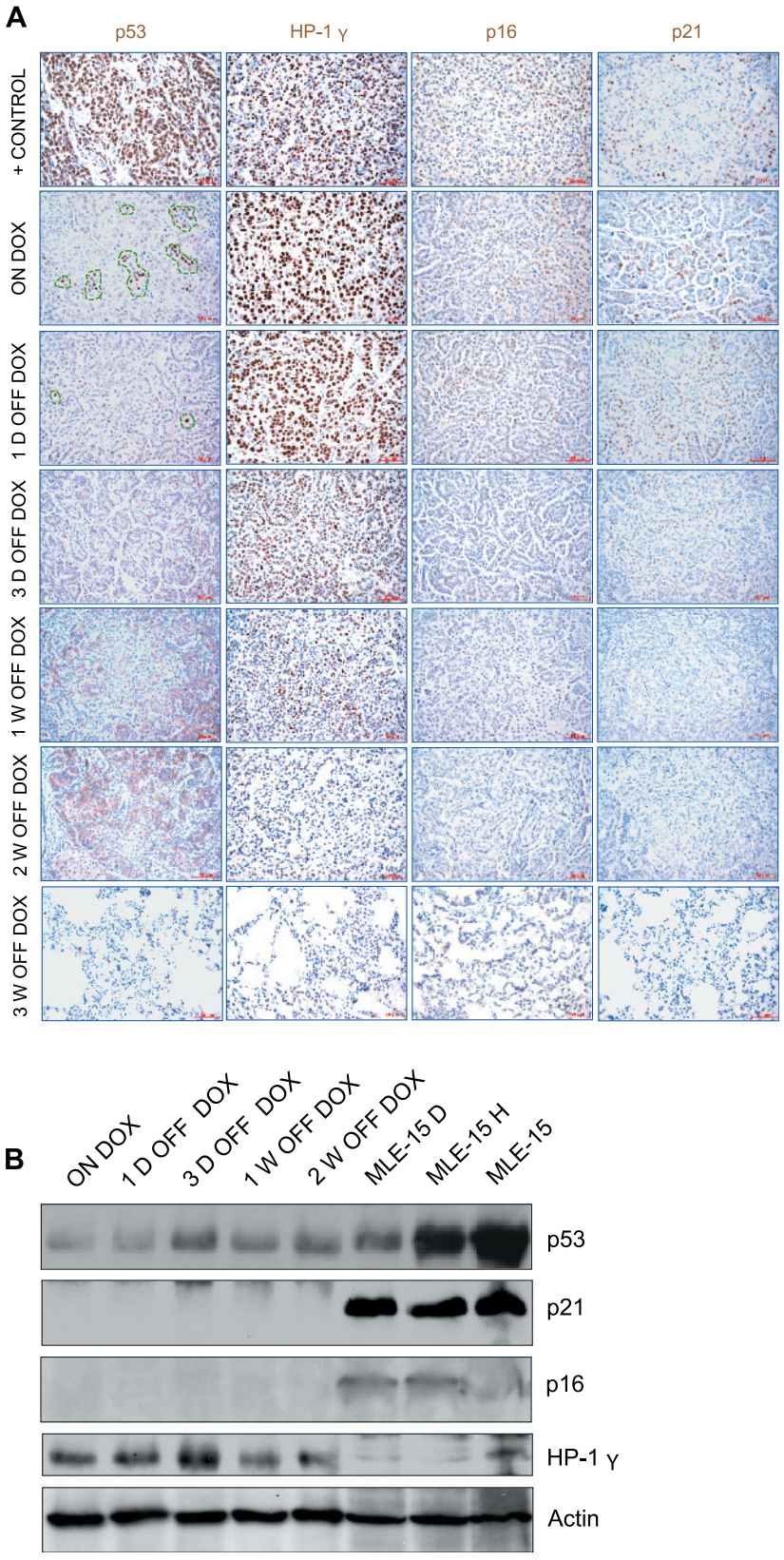

Figure W16. Deinduction of oncogenic C-RAF in lung tumors of DTR^{S} mice leads to reduction in senescence-associated markers. (A) Immunohistochemical analysis of lung tumor sections for the indicated proteins. Hematoxylin (blue) was used as a counterstain for immunohistochemistry. For p53 staining, tumor section of a xenograph generated by subcutaneous injection of mouse MLE-15 NSCLC was used as a positive control. For HP-1γ, p16, and p21 immunohistochemistry, lung tumor sections from K-*ras*^{LA2} mouse were used as a positive control. Circled regions represent tumor cells with nuclear p53 staining. (B) Immunoblot analysis of lung tumor lysates from induced or DOX-removed DTR^{S} mice for indicated markers. MLE-15 D indicates MLE-15 cells treated with doxorubicin hydrochloride; MLE-15 H, MLE-15 cells treated with cycloheximide.

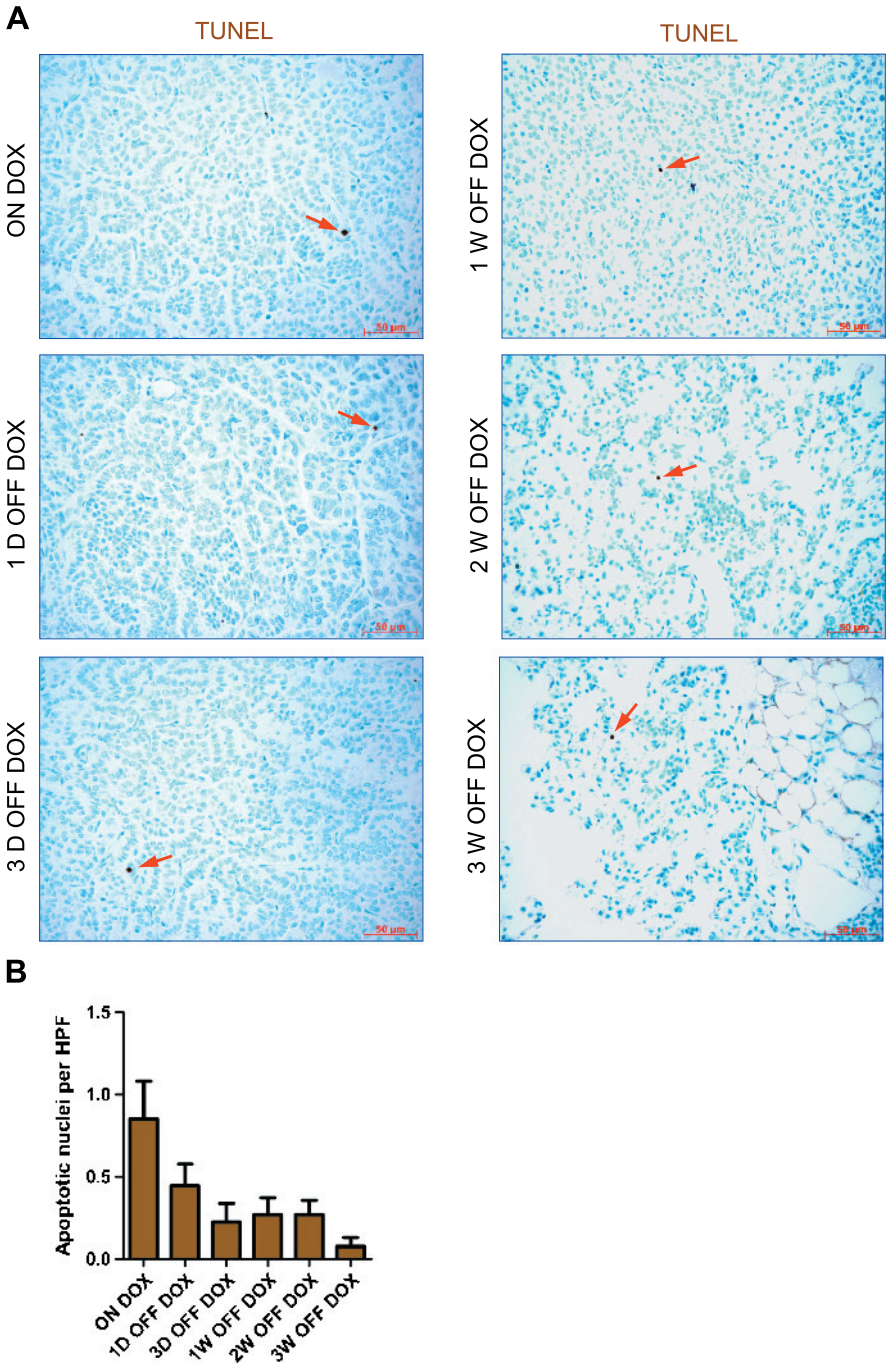

Figure W17. DOX withdrawal from oncogenic C-RAF–driven lung tumors does not lead to increased apoptosis. (A) Sections of lung tumors from DTR^S mice for the indicated DOX schedules were assayed for apoptotic cells using the TdT-mediated dUTP nick end labeling (TUNEL) procedure. Examples of TUNEL-positive cells are indicated by red arrows. (B) Quantification of TUNEL-positive cells/high-power field (HPF). Error bars are SEM from three different mice for each category.

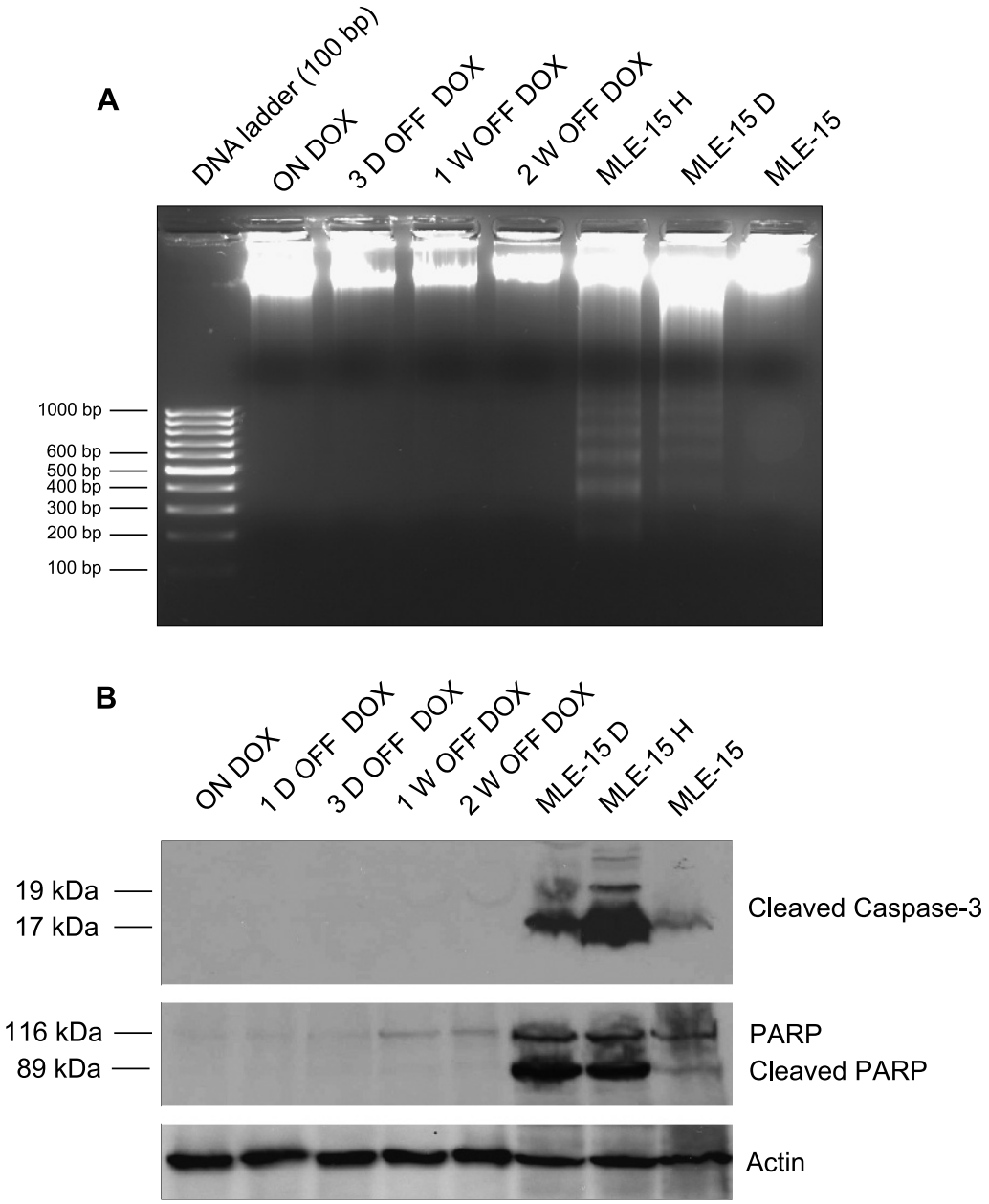

Figure W18. Absence of apoptosis in oncogenic C-RAF–driven lung tumors after deinduction. (A) Analysis of genomic DNA fragmentation in induced lung tumors removed from DOX for the indicated time points. About 1.5 μg of DNA was separated by electrophoresis on a 2% agarose gel. A 100-bp marker was used for determining the size of the DNA fragments. MLE-15 cells that were treated either with doxorubicin hydrochloride (MLE-15 D) or cycloheximide (MLE-15 H) and show DNA fragmentation compared to parental MLE-15 cells were used as positive controls. (B) Cleavage of caspase-3 and PARP expression in control and deinduced lung tumor lysates by Western blot analysis. Actin was used as a loading control.

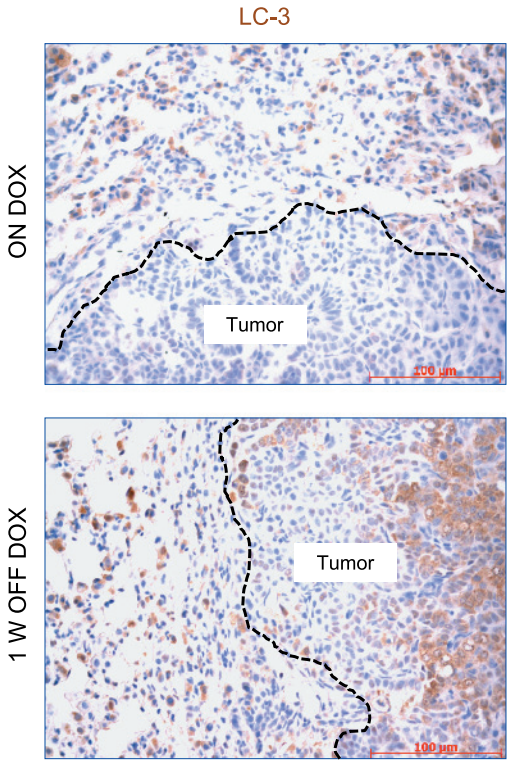

Figure W19. Oncogenic C-RAF–driven lung tumors display lower autophagic capacity than their surrounding nontumor regions. Immunohistochemical analysis of lung tumor sections from DOX-induced and deinduced DTR^{S} mice for LC-3. Hematoxylin (blue) was used as a counterstain for immunohistochemistry.

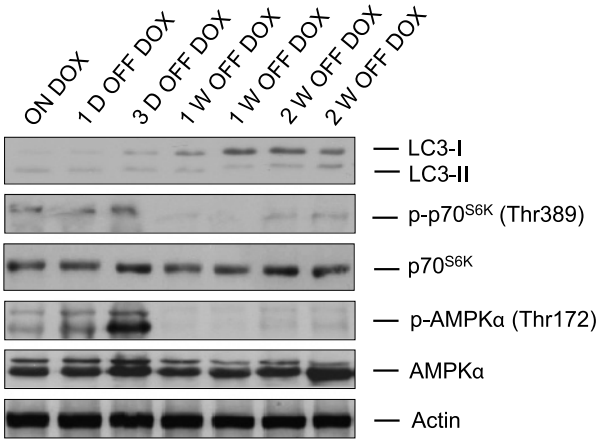

Figure W20. Inhibition of mTOR signaling in regressing lung tumors does not correlate with AMPK activation. Immunoblot analysis of lung tumor lysates from induced or DOX-removed DTR^{S} mice for the indicated markers. Actin was used as a loading control.